



Deactivation of Pd/Ce_{0.5}Zr_{0.5}O₂ model three-way catalyst by P, Ca and Zn deposition

S.Y. Christou^a, S. García-Rodríguez^b, J.L.G. Fierro^b, A.M. Efstathiou^{a,*}

^a Department of Chemistry, Heterogeneous Catalysis Laboratory, University of Cyprus, P.O. Box 20537, CY 1678 Nicosia, Cyprus

^b Instituto de Catálisis y Petroleoquímica (CSIC), Marie Curie 2, Cantoblanco, 28049-Madrid, Spain

ARTICLE INFO

Article history:

Available online 8 October 2011

Keywords:

“Three-way” catalyst
Catalyst deactivation
P, Ca and Zn chemical poisoning
Oxygen storage capacity
OSC
CO oxidation
C₃H₆ oxidation
NO reduction

ABSTRACT

The negative effects of P, P-Ca and P-Zn deposition on the surface of a model 1 wt% Pd/Ce_{0.5}Zr_{0.5}O₂ “three-way” catalyst (TWC) on its structural, morphological, textural, oxygen storage and release, and catalytic performance have been investigated for the first time. The aim of this research work is to provide fundamental understanding on the multiple functions of a TWC when P, Ca and Zn contaminants are accumulated on its surface. Towards this aim, a model Pd/Ce_{0.5}Zr_{0.5}O₂ TWC and P, P-Ca and P-Zn contaminated ones were prepared and characterised by means of BET, XRD, HR-TEM, XPS and H₂/O₂ pulse injection techniques. The catalytic performance of the non-contaminated and contaminated Pd/Ce_{0.5}Zr_{0.5}O₂ solids was evaluated for CO and C₃H₆ oxidation and NO reduction by H₂ probe reactions under oxygen lean conditions. Incorporation of P, Ca and Zn contaminants was found to cause a significant decline (16–40%) in the concentration (μmol O/g) of labile active (OSC) and total (OSCC) oxygen species of Pd/Ce_{0.5}Zr_{0.5}O₂ catalyst aged in air at 850 °C. After P incorporation followed by calcination at 850 °C, CePO₄ was detected, while in the presence of Ca or Zn the formation of Ca₃(PO₄)₂ and ZnO, respectively, was verified. At low reaction temperatures, co-addition of Zn and P was found to further deteriorate the OSC (μmol O/g), while at high temperatures no appreciable differences were observed. This is ascribed to the formation of CePO₄ which decreases significantly the degree of reduction of Ce(IV) oxide. CePO₄ physically covers catalyst particles (e.g., pore mouth and internal surface) leading to the substantial loss of BET area, pores volume, and Pd surface sites. More importantly, it is shown for the first time that the presence of Pd was found to diminish to a great extent the deteriorating effect of P, Ca and Zn when deposited on Ce_{0.5}Zr_{0.5}O₂ on its oxygen storage and release properties. High concentrations (mg/g) of P, P-Ca and P-Zn contaminants on the catalyst surface was found to cause a considerable decrease in catalyst's activity for CO and C₃H₆ oxidation, and NO reduction by H₂ under oxygen lean conditions. The deterioration of catalytic performance is largely due to the presence of P, and to a lesser extent to the presence of Ca or Zn.

© 2011 Elsevier B.V. All rights reserved.

1. Introduction

Nowadays, “three-way” catalysts (TWCs) installed in gasoline-powered vehicle emission control systems for simultaneous conversion of carbon monoxide (CO), nitrogen oxides (NO_x) and unburnt hydrocarbons (HCs) comprise the state-of-the-art gas after-treatment technology. TWCs must maintain enhanced catalytic performance under the dynamic conditions they operate during their entire life cycle, showing advanced poison tolerance and thermal durability. However, under the conditions catalytic converters are frequently subjected to during real driving conditions, they progressively experience structural and morphological changes caused by thermal, mechanical and chemical deactivation,

and, therefore, fail to meet the continually stringent required emissions standards [1–5].

The loss of catalytic activity and/or selectivity of TWCs over time are of crucial importance. Chemical poisoning along with high-temperature thermal aging constitute the main reasons of TWCs deactivation [1–5]. Chemical deactivation involves physical blockage and surface rearrangement due to the binding of the active catalytic sites by impurities present in the exhaust gas, the sources of which being the fuel, lubricant oil additives, and exhaust pipe components [6–9]. The most serious deactivating effects are due to phosphorus [7,10–12], lead [13–15] and sulfur [16,17] accumulated in the TWC. Nevertheless, the reduction of sulfur levels and the use of unleaded gasoline taken as control measures by the developed countries as part of their environmental policy have led to the partial confrontation of the problem.

Accumulation of contaminants on the surface of “three-way” catalysts was the subject of many studies [4,8,18–20] since it is one of the main causes of their deactivation. Phosphorus has

* Corresponding author. Tel.: +357 22 892776; fax: +357 22 892801.

E-mail address: efstath@ucy.ac.cy (A.M. Efstathiou).

been detected in aged commercial TWCs in the form of a glassy overlayer formed on the washcoat surface, constituting mainly of $(\text{Zn,Ca,Mg})_3(\text{PO}_4)_2$ type phosphates, or other phosphate compounds formed upon reaction with washcoat components, such as CePO_4 , $\text{Ce}(\text{PO}_3)_3$ and AlPO_4 [7,11,21–23]. Larese et al. [12,24] compared fresh and aged commercial “three-way” catalysts, the latter extracted from the exhaust pipe of a gasoline-driven car. They reported that the formation of CePO_4 was detrimental to the TWC activity, where the $\text{Ce}^{3+}/\text{Ce}^{4+}$ pair is locked and unable to participate in the $\text{Ce}^{3+} \leftrightarrow \text{Ce}^{4+}$ redox process required for the proper functioning of TWC. Although P-poisoning has been extensively studied, most of the fundamental studies carried out were focused on the effects caused after P is deposited on the surface of ceria or ceria–zirconia support materials [25–27]. However, the role of these contaminants in the deactivation of TWCs is not yet fully understood. Only very few studies were focused on the individual or combined effects of chemical poisons on the oxygen storage and catalytic properties of TWCs. Kröger et al. [28] studied the effect of P and Ca on the catalytic activity of a supported-Rh catalyst, where it was found that the deactivating effect of Ca was not as strong as that of P. The studies of Tabata et al. [14,15] on model Zn-, Fe-, and Pb-poisoned catalysts showed that only Pb caused a considerable decrease in the activity and selectivity of NO reduction. Heo et al. [29] investigated field-aged Pd-based TWCs and indicated that sintering of noble metal and degradation of OSC resulted in a gradual decrease of activity in CO oxidation.

In a recent work from our laboratory [30] regarding the effects of P, Ca and/or Zn poisons on the oxygen storage and release properties of a $\text{Ce}_{0.5}\text{Zr}_{0.5}\text{O}_2$ solid solution, it was found that calcium and zinc were mainly concentrated on the surface of the $\text{Ce}_{0.5}\text{Zr}_{0.5}\text{O}_2$ solid material, causing a significant increase in the activation energy (kcal/mol) of surface oxygen diffusion. On the contrary, phosphorus penetrated deeper within the solid particles and interacted with cerium oxide forming cerium phosphate. This was found to result in a substantial suppression of the bulk oxygen diffusion kinetics [30].

The present work attempts for the first time to unveil the degree of deactivation of a model 1 wt% Pd/ $\text{Ce}_{0.5}\text{Zr}_{0.5}\text{O}_2$ “three-way” catalyst induced by phosphorous, calcium and/or zinc chemical poisoning. For this purpose, P (4.5 wt%), Ca (1.0 wt%) and/or Zn (1.0 wt%) poisons were deposited on the surface of a 1 wt% Pd/ $\text{Ce}_{0.5}\text{Zr}_{0.5}\text{O}_2$ solid by the wet impregnation method. The investigation was focused on the modification of the structural, morphological, textural, OSC and catalytic properties of the Pd/ $\text{Ce}_{0.5}\text{Zr}_{0.5}\text{O}_2$ solid caused by contamination with P, P-Ca and P-Zn. The contaminants were found to be deposited on the catalyst surface largely in the form of CePO_4 , $\text{Ca}_3(\text{PO}_4)_2$ and ZnO , causing also physical blockage of its pores structure with substantial reduction in BET surface area ($\text{m}^2 \text{ g}^{-1}$) and Pd surface sites. Deposition of P, P-Ca and P-Zn contaminants on the Pd/ $\text{Ce}_{0.5}\text{Zr}_{0.5}\text{O}_2$ catalyst surface was found to considerably deteriorate its oxygen storage capacity and catalytic activity in CO and C_3H_6 oxidation, and NO reduction by H_2 under lean oxygen reaction conditions. The presence of Pd on the surface of $\text{Ce}_{0.5}\text{Zr}_{0.5}\text{O}_2$ solid solution was found to significantly enhance the oxygen storage process in the presence of P, Ca and/or Zn poisons, preventing catalyst deactivation to a large degree, as compared to the Pd-free solid support material.

2. Experimental

2.1. Synthesis of fresh and contaminated with P, P-Ca and P-Zn Pd/ $\text{Ce}_{0.5}\text{Zr}_{0.5}\text{O}_2$ catalysts

The $\text{Ce}_{0.5}\text{Zr}_{0.5}\text{O}_2$ (50 mol% CeO_2 and 50 mol% ZrO_2) support material was synthesized using a commercial proprietary

co-precipitation method (MEL Chemicals, UK) and calcined in air at 850 °C for 4 h. After that, it was impregnated with $\text{Pd}(\text{NO}_3)_2$ (Aldrich, 99.999%) solution in distilled de-ionized water at 60 °C in order to yield 1 wt% of metal nominal loading. The supported Pd/ $\text{Ce}_{0.5}\text{Zr}_{0.5}\text{O}_2$ catalyst was calcined in air at 500 °C for 2 h (fresh). To prepare the P, P-Ca and P-Zn contaminated Pd/ $\text{Ce}_{0.5}\text{Zr}_{0.5}\text{O}_2$ solids, equal amounts of the supported catalyst were impregnated with solutions containing appropriate amounts of $\text{NH}_4\text{H}_2\text{PO}_4$, $\text{Ca}(\text{NO}_3)_2 \cdot 4\text{H}_2\text{O}$ and $\text{Zn}(\text{NO}_3)_2 \cdot 6\text{H}_2\text{O}$ precursor salts corresponding to P, Ca and Zn loadings of 4.5, 1.0 and 1.0 wt%, respectively. These contaminant loadings are within the range detected in aged commercial TWCs [6,9,12,20]. Prior to any OSC or catalytic activity measurements, and any characterisation studies, the contaminated with P, P-Ca or P-Zn Pd/ $\text{Ce}_{0.5}\text{Zr}_{0.5}\text{O}_2$ solids were calcined in air at 850 °C for 4 h. For comparison purposes, a fraction of the fresh 1 wt% Pd/ $\text{Ce}_{0.5}\text{Zr}_{0.5}\text{O}_2$ catalyst was also subjected to thermal aging in air at 850 °C for 4 h (aged catalyst).

2.2. X-ray diffraction (XRD) analysis

Powder X-ray diffraction (XRD) patterns of non-contaminated and contaminated with P, P-Ca or P-Zn supported Pd/ $\text{Ce}_{0.5}\text{Zr}_{0.5}\text{O}_2$ catalysts were recorded in the 10–80 °C 2θ range (scan speed = 0.02°/s, step = 0.02°) using a Shimadzu 600 Series Diffractometer and after employing $\text{CuK}\alpha$ radiation ($\lambda = 1.5418 \text{ \AA}$) with high-precision angle reproducibility ($\pm 0.001^\circ$ 2θ) and DS, SS and RS slit widths equal to 1.0°, 1.0° and 0.3 mm, respectively, in a continuous scan mode.

2.3. BET specific surface area and pores volume measurements

BET specific surface area and pores volume measurements were performed on the prepared solid catalysts by N_2 adsorption–desorption isotherms at –196 °C using a Micromeritics Gemini Surface Area and Pore Size Analyser. Prior to measurements the samples were degassed at 300 °C for 2 h in pure N_2 gas flow.

2.4. Transmission electron microscopy (TEM) studies

Samples in powder form were reduced in 25 mL/min H_2 flow at 300 °C for 2 h in a quartz reactor. Afterwards, the sample was left to cool down in H_2 flow and then purged in He flow before transferred to the TEM instrument. Samples were then dispersed in ethanol in an ultrasonic bath. A few drops of the dispersed solution were deposited on the lacey carbon-coated copper grids for TEM observation. A 200 kV TEM/STEM 2100-F transmission electron microscope (Jeol Ltd.) was used to record TEM, HR-TEM and STEM images. X-ray energy dispersive spectroscopy (EDS) analyses were performed with an Oxford INCAx-Sight EDS detector coupled to the microscope. STEM images were acquired using a 1-nm electron probe and an annular dark field detector with an inner collection angle of 59 mrad. Z-contrast can be observed in High Angle Annular Dark Field (HAADF) STEM images at constant sample width. EDS spectra were analysed using the INCA Microanalysis Suite software. Quantification was performed by integration of the following X-ray energy lines: Pd-L, Ce-L, Zr-L, O-K, Zn-K, P-K and Ca-K.

2.5. Hydrogen temperature-programmed desorption (H_2 -TPD) studies

The Pd surface sites available for H_2 chemisorption over the Pd/ $\text{Ce}_{0.5}\text{Zr}_{0.5}\text{O}_2$ and the P, P-Ca or P-Zn contaminated ones were estimated by H_2 -TPD in a specially designed gas flow-system previously described [31]. The fresh catalyst sample (100 mg) was first treated *in situ* in a flow of 20 vol% O_2/He gas mixture at 500 °C for

2 h, and then reduced in pure H₂ (1 bar) at 300 °C for 2 h. The catalyst was then purged in He at 500 °C until no H₂ evolution was observed, and then cooled quickly to 30 °C. A 1 vol% H₂/He (30 NmL/min) gas mixture were then passed over the catalyst for 30 min followed by a switch to He flow. At the same time, the temperature of the catalyst bed was increased to 700 °C to carry out a TPD run.

2.6. X-ray photoelectron spectroscopy (XPS) studies

X-ray photoelectron spectroscopy (XPS) studies were performed using a VG Escalab 200R spectrometer equipped with a hemispherical electron analyzer and a Mg-K α (1253.6 eV) X-ray source. XP spectra were recorded after the samples were reduced at 300 °C for 2 h in pure H₂, and after oxidation at 500 °C for 2 h in 20%O₂/Ar gas mixture. Prior to analysis the samples were degassed under high vacuum for 15 min before transferred to the analysis chamber. The procedure followed for processing the XP spectra recorded has been previously described [9,32]. The error in estimating surface composition and atom ratios from XPS data is considered to be less than 10%.

2.7. Oxygen storage capacity (OSC) measurements

The oxygen storage capacity of the fresh, aged and contaminated Pd/Ce_{0.5}Zr_{0.5}O₂ solids with P, P-Ca and P-Zn was measured in the 550–850 °C range by using the H₂/O₂ pulse injection technique [33]. The concentration of the most reactive labile oxygen species of the catalyst, named “Oxygen Storage Capacity (OSC)” is defined as the amount of oxygen (μmol O g⁻¹) that reacts off during the first H₂ pulse. The “Oxygen Storage Capacity Complete (OSCC)” of the solid is defined as the total concentration (μmol O g⁻¹) of oxygen species that reacts with several consecutive pulses of H₂ (until no hydrogen consumption is seen). OSCC is calculated based on the amount of oxygen consumed during the re-oxidation stage of the pulse experiment following H₂ pulse(s), and not based on H₂ consumption or H₂O formation. For the former, an overestimation of OSC due to hydrogen dissolution into the bulk of Pd and support solid phases could have been arisen. Oxygen consumption was calculated based on the difference in the area of the oxygen pulse bypass and through the reactor. H₂ instead of CO was used as a reducing agent since the use of CO is accompanied by a complicated reaction scheme involving the disproportionation reaction and the formation of carbonate species on the support, which make the estimation of the net oxygen storage capacity more difficult [34]. The apparatus and experimental protocol used for OSC measurements were reported in detail elsewhere [34].

2.8. Catalytic activity measurements

The gas flow-system used for conducting catalytic measurements for the 1 vol% CO/0.2 vol% C₃H₆/1 vol% O₂/He and 0.1 vol% NO/0.3 vol% H₂/1 vol% O₂/He model reactions at 1 atm total pressure was previously described [31]. The total flow rate was 100 NmL min⁻¹. Prior to all measurements, the sample ($W_{\text{cat}} = 0.1$ g) was first treated in a flow of 20 vol% O₂/He gas mixture for 2 h at 500 °C, followed by reduction in H₂ (1 atm) flow at 300 °C for 2 h. The catalyst was then cooled in He flow to 30 °C, the feed was switched to the reaction gas mixture, and the temperature of the catalyst was then increased to 700 °C at the rate of 30 °C/min to carry out a temperature-programmed surface reaction (TPSR) experiment. The exit product gas from the micro-reactor was continuously monitored by *on line* mass spectrometer (Omnistar, 1–300 amu, Balzers). The mass numbers (m/z) of 2, 18, 28, 30, 32, 42, and 44 were used for H₂, H₂O, CO, NO, O₂, C₃H₆ and CO₂ (or N₂O), respectively. The conversions of CO (X_{CO} , %), C₃H₆ (X_{C3H6} , %) and NO (X_{NO} , %) were estimated based on the signals recorded at the m/z of 28, 42

and 30, respectively. For the correct estimation of the concentration (ppm or mol%) of reaction products, the prepared feed gas mixture was passed bypass the reactor in order to record the background signal of a given m/z corresponding to a given reaction product in the mass spectrometer in the presence of the other gases, and not only in He diluent gas. Sensitivity (MS signal/ppm) and cracking coefficients of a given component required for the conversion of the corresponding m/z signal to concentration (ppm or mol%) were determined based on a calibration mixture of that component in He diluent gas. Corrections in the sensitivity of a given gas component obtained in He diluent due to the presence of other gases in the reaction mixture were made, if necessary. For example, the contribution of CO₂ ($m/z = 44$) to $m/z = 28$ (CO), and that of N₂O ($m/z = 44$) to $m/z = 30$ (NO) were taken into account. Details of the mass spectrometry analysis of the reactor gas effluent performed in the case of the deNO_x reaction investigated have been reported previously [35].

3. Results and discussion

3.1. Structural, textural and morphological characterisation of the non-contaminated and contaminated with P, P-Ca and P-Zn Pd/Ce_{0.5}Zr_{0.5}O₂ catalysts

The structural, morphological and textural properties of 1 wt% Pd/Ce_{0.5}Zr_{0.5}O₂, P-Pd/Ce_{0.5}Zr_{0.5}O₂, P-Ca-Pd/Ce_{0.5}Zr_{0.5}O₂, and P-Zn-Pd/Ce_{0.5}Zr_{0.5}O₂ solids were investigated by XRD, BET, TEM and H₂-TPD techniques, where results are presented and discussed in what follows.

3.1.1. Structural characterisation—XRD studies

Fig. 1a compares the powder XRD patterns of the non-contaminated Pd/Ce_{0.5}Zr_{0.5}O₂ solid before (fresh) and after calcination at 850 °C (aged), while Fig. 1b compares the XRD patterns of the fresh non-contaminated Pd/Ce_{0.5}Zr_{0.5}O₂ solid and the contaminated with P, P-Ca and P-Zn Pd/Ce_{0.5}Zr_{0.5}O₂ solids after calcination at 850 °C (Section 2.1). As seen in Fig. 1a, the XRD pattern of Pd/Ce_{0.5}Zr_{0.5}O₂ exhibits the main diffraction peaks corresponding to (111), (200), (220), (311) and (222) planes of the cubic phase fluorite-type (Fm3m) structure of CeO₂ (■) at $2\theta = 29.24$, 33.82, 48.66, 57.78 and 60.62°, respectively [36,37]. No PdO phase was observed in any of the XRD diffractograms recorded for the Pd/Ce_{0.5}Zr_{0.5}O₂ catalysts due to the low Pd loading (1 wt%) and the presence of PdO particles with a mean particle size of less than 3.0 nm. The XRD pattern of Ce_{0.5}Zr_{0.5}O₂ mixed oxide showed the presence of only a single phase solid solution with pseudocubic or tetragonal structure, suggesting that Ce⁴⁺ and Zr⁴⁺ cations are highly homogeneously distributed in the lattice; the smaller in size Zr⁴⁺ (0.84 Å) cations have replaced isovalent Ce⁴⁺ (0.97 Å) cationic sites in the ceria lattice. However, it is known that the broadness of the XRD peaks does not allow the unequivocal assignment of the obtained pattern to a tetragonal or cubic phase [36,37]. After aging of the catalyst (Section 2.1), it was found that this mainly retains the pseudo-cubic structure with only a very weak evidence of phase segregation accompanied by the formation of a CeO₂-rich phase, as might be seen by the appearance of a small peak broadening; a shoulder at low 2θ for the (311) reflection is pointed out by an arrow in Fig. 1a. On the other hand, the maximum intensity of the diffraction peaks was found to slightly increase, thus demonstrating the further growth of the crystal grain after calcination at 850 °C. The primary crystallite size of the fresh sample was estimated from the diffraction pattern using the Scherrer equation, where it was found to increase from 6.6 to 7.3 ± 0.1 nm (Table 1) after increasing the thermal treatment from 500 to 850 °C in 20 vol% O₂/He (aged sample).

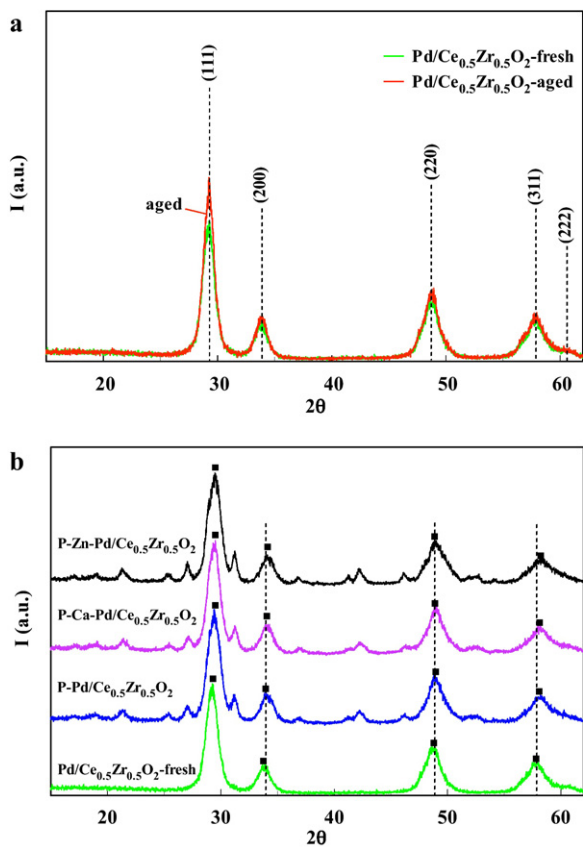


Fig. 1. Powder XRD patterns of the fresh and aged non-contaminated (a) and P, P-Ca and P-Zn contaminated (b) $\text{Pd}/\text{Ce}_{0.5}\text{Zr}_{0.5}\text{O}_2$ catalysts (cubic $\text{Ce}_x\text{Zr}_{1-x}\text{O}_2$: ■, CePO_4 : *).

It becomes obvious from the results of Fig. 1b that in addition to the main diffraction peaks due to the cubic $\text{Ce}_{0.5}\text{Zr}_{0.5}\text{O}_2$ solid solution, the contaminated solids display also several weak but clearly visible diffraction peaks (marked with *), which are ascribed to CePO_4 monazite (JCPDS 32-0199) [11,25,26,38]. The formation of $\text{Ca}_3(\text{PO}_4)_2$ or $\text{Zn}_3(\text{PO}_4)_2$ in the doubly poisoned samples could not be verified by XRD analysis due to their low concentrations. Similar observations were also made in a previous study concerning the chemical poisoning of the same $\text{Ce}_{0.5}\text{Zr}_{0.5}\text{O}_2$ solid by P, Ca and Zn [30], as well as after P was deliberately incorporated in CeO_2 and $\text{Ce}_x\text{Zr}_{1-x}\text{O}_2$ solids [25,26,28]. Asymmetric broad shaped peaks exhibited by the poisoned samples can be related to poor crystallinity. Fig. 1b also shows that after contamination small phase segregation does occur with the formation of a ZrO_2 -rich solid phase, as indicated by the broadening and some splitting of the peaks in the $\text{Ce}_{0.5}\text{Zr}_{0.5}\text{O}_2$ pattern (shoulders at high 2θ for the (200), (220) and (311) reflections pointed out by arrows), which implies that phase de-mixing is favoured in the presence of

Table 2

BET specific surface area ($\text{m}^2 \text{g}^{-1}$) and specific pores volume ($\text{cm}^3 \text{g}^{-1}$) obtained over the fresh and aged non-contaminated, and P, P-Ca or P-Zn contaminated $\text{Pd}/\text{Ce}_{0.5}\text{Zr}_{0.5}\text{O}_2$ catalysts (aged).

Catalyst	BET area ($\text{m}^2 \text{g}^{-1}$)	Specific pores volume ($\text{cm}^3 \text{g}^{-1}$)
$\text{Pd}/\text{Ce}_{0.5}\text{Zr}_{0.5}\text{O}_2$ -fresh	50.6	0.178
$\text{Pd}/\text{Ce}_{0.5}\text{Zr}_{0.5}\text{O}_2$ -aged ^a	35.6	0.159
$\text{P-Pd}/\text{Ce}_{0.5}\text{Zr}_{0.5}\text{O}_2$ -aged	25.2	0.108
$\text{P-Ca-Pd}/\text{Ce}_{0.5}\text{Zr}_{0.5}\text{O}_2$ -aged	22.3	0.063
$\text{P-Zn-Pd}/\text{Ce}_{0.5}\text{Zr}_{0.5}\text{O}_2$ -aged	16.8	0.056

^a Calcination in air at 850 °C for 4 h (Section 2.1).

P, Ca or Zn poisons. The lattice parameters estimated from XRD data using the Rietveld analysis of diffraction profile fitting for the non-contaminated and contaminated $\text{Pd}/\text{Ce}_{0.5}\text{Zr}_{0.5}\text{O}_2$ solids, assuming a cubic cell environment for the $\text{Ce}_{0.5}\text{Zr}_{0.5}\text{O}_2$ solid, are listed in Table 1. The α value of 5.29 Å obtained for the $\text{Ce}_{0.5}\text{Zr}_{0.5}\text{O}_2$ -fresh solid is compared reasonably well with that reported in the literature for a solid solution of similar composition [35,36]. The lower crystallinity observed over the phosphated samples along with the increased inhomogeneity appear to result in a small decrease of the mean primary crystallite size (Table 1, last column).

3.1.2. Textural characterisation—BET specific surface area and pores volume

Table 2 summarizes the BET specific surface area ($\text{m}^2 \text{g}^{-1}$) and pores volume ($\text{cm}^3 \text{g}^{-1}$) measured over the fresh and aged $\text{Pd}/\text{Ce}_{0.5}\text{Zr}_{0.5}\text{O}_2$ solids, and those contaminated with P, P-Ca and P-Zn elements (aged at 850 °C). It is worth pointing out that deposition of Pd on the surface of $\text{Ce}_{0.5}\text{Zr}_{0.5}\text{O}_2$ support (BET = 52.5 $\text{m}^2 \text{g}^{-1}$; specific pores volume = 0.235 $\text{cm}^3 \text{g}^{-1}$) resulted in a small decrease of the surface area and to a greater extent of the pores volume (Table 2). On the other hand, chemical poisoning results in a significant reduction of the BET area of $\text{Pd}/\text{Ce}_{0.5}\text{Zr}_{0.5}\text{O}_2$ -aged solid to about 30–53% of its initial value. The greatest loss was observed after deposition of P-Zn. Addition of P-Ca appears not to result in additional deterioration of the BET surface area compared to that caused by P deposition alone. It should be noticed that in the absence of contaminants calcination of $\text{Pd}/\text{Ce}_{0.5}\text{Zr}_{0.5}\text{O}_2$ catalyst in air at 850 °C for 4 h (aged sample) resulted in the decrease of BET surface area from 50.6 (calcination in air at 500 °C, 2 h) to 35.6 $\text{m}^2 \text{g}^{-1}$ (30% reduction). This loss in the surface area of the catalysts has been found to be associated with changes in the pores structure occurring in two stages [5,39]. At first, crystallite growth takes place which is considered as a pre-sintering phenomenon, followed by agglomeration among crystallites. The aging procedure employed appears to induce structural transformations as revealed by the decrease of the pores volume of support material. However, after thermal aging of the $\text{Pd}/\text{Ce}_{0.5}\text{Zr}_{0.5}\text{O}_2$ solid only 10% of its initial pores volume was lost, while P-poisoning resulted in ~40% decrease in pores volume. In the case of the doubly poisoned (P-Ca or P-Zn) $\text{Pd}/\text{Ce}_{0.5}\text{Zr}_{0.5}\text{O}_2$ solids, these were found to possess even smaller pores volumes (65–69% loss) when compared to the fresh one. The formation of $\text{Ca}_3(\text{PO}_4)_2$ powdery salt which accumulates on the surface of support is most likely the cause of the observed alterations in the textural properties of P-Ca-Pd/ $\text{Ce}_{0.5}\text{Zr}_{0.5}\text{O}_2$. Amorphous glaze-like Ca phosphate, which is difficult to reverse, has been detected in aged TWCs, causing fouling by physical blockage of catalyst pores mouth [12,21]. Phosphate salts derived from lubricant oil additives were found to form an overlayer on the catalyst surface causing masking or blockage of micropores, which explains the loss in BET specific surface area and pores volume [22,40].

Table 1

Lattice parameters and primary crystallite size of $\text{Ce}_{0.5}\text{Zr}_{0.5}\text{O}_2$ support for the non-contaminated fresh and aged, and contaminated with P, P-Ca or P-Zn $\text{Pd}/\text{Ce}_{0.5}\text{Zr}_{0.5}\text{O}_2$ catalysts.

Catalyst	d (111) (Å)	α (Å)	Cell volume (Å ³)	Primary crystallite size (nm)
$\text{Pd}/\text{Ce}_{0.5}\text{Zr}_{0.5}\text{O}_2$ -fresh ^a	3.052	5.29	147.6	6.6 ± 0.1
$\text{Pd}/\text{Ce}_{0.5}\text{Zr}_{0.5}\text{O}_2$ -aged ^b	3.049	5.28	147.3	7.3 ± 0.2
$\text{P-Pd}/\text{Ce}_{0.5}\text{Zr}_{0.5}\text{O}_2$ -aged	3.034	5.25	145.1	6.0 ± 0.1
$\text{P-Ca-Pd}/\text{Ce}_{0.5}\text{Zr}_{0.5}\text{O}_2$ -aged	3.035	5.26	145.2	6.4 ± 0.1
$\text{P-Zn-Pd}/\text{Ce}_{0.5}\text{Zr}_{0.5}\text{O}_2$ -aged	3.032	5.25	144.8	5.9 ± 0.1

^a Calcination in air at 500 °C for 2 h (Section 2.1).

^b Calcination in air at 850 °C for 4 h (Section 2.1).

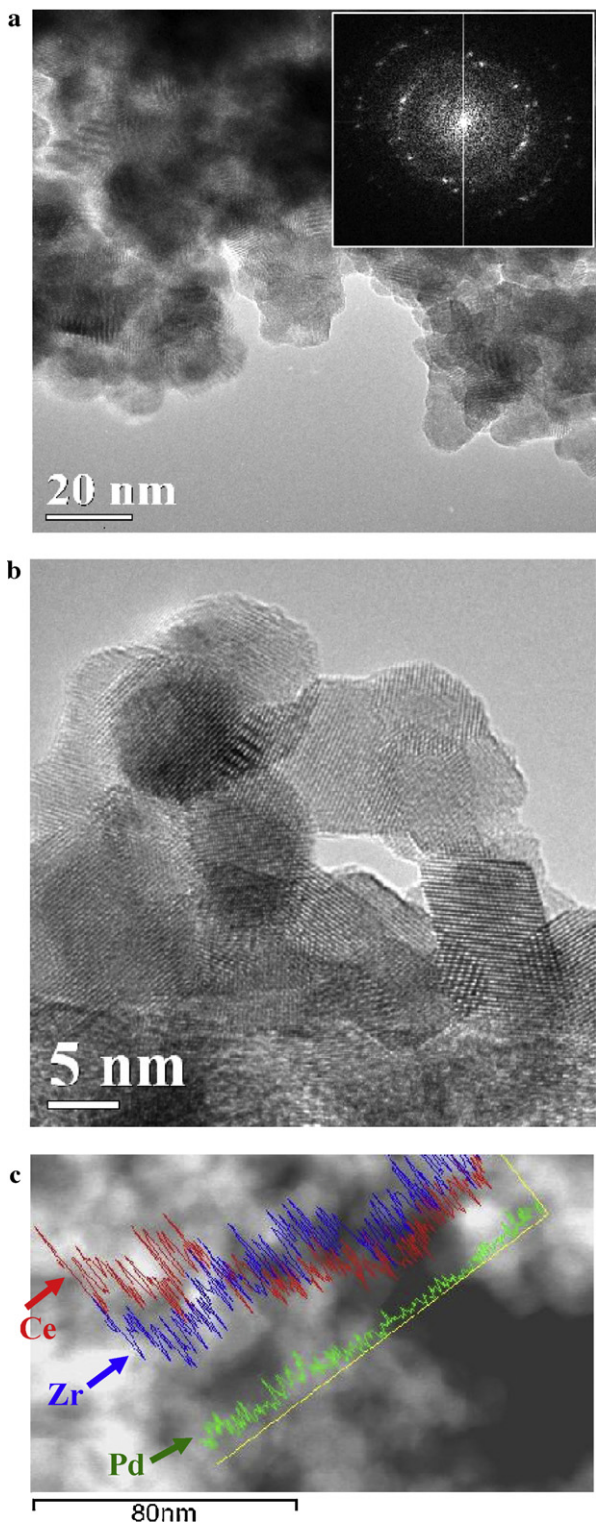


Fig. 2. (a) TEM image (the inset shows the digital diffraction pattern of the image); (b) HRTEM image; and (c) HAADF-STEM image with Ce- $\text{L}\alpha_1$, Zr- $\text{L}\alpha_1$, and Pd- $\text{L}\alpha_1$ X-ray energy line profiles obtained over the Pd/Ce_{0.5}Zr_{0.5}O₂ catalyst.

3.1.3. Morphological characterisation—TEM studies

Fig. 2a and b shows TEM images of the Pd/Ce_{0.5}Zr_{0.5}O₂ catalyst at a low (20 nm scale unit) and high (5 nm scale unit) magnification, respectively. The size of Ce_{0.5}Zr_{0.5}O₂ particles range between 5 and 10 nm, in good agreement with the crystallite size estimated from XRD measurements (Table 1). The image depicted in Fig. 2b shows that the sample is composed of sphere-like nanoparticles.

The inset in Fig. 2a is a digital diffraction pattern of the image indicating the high crystallinity of these particles. Individual Pd particles could not be detected in the HR-TEM images due to the combined effect of small Pd particle size and the high crystallinity of the support, which renders difficult the phase contrast between the Pd particles and the support (Fig. 2a and b). STEM mode was used to perform several point and profile EDS analyses in order to identify possible regions where Pd were agglomerated. Pd was found to be homogeneously distributed according to the EDS profiles (Fig. 2c). Although image contrast in STEM mode is related to the Z number in the sample, individual Pd particles were not identified in HAADF-STEM images because the atomic numbers of Pd and the atoms of support are close to each other and do not generate enough Z-contrast to be correctly imaged. Although metal particles in the size of 1 nm supported on low-surface area carriers have been imaged in HR-TEM mode by Bernal et al. [41,42], the small size of the present Ce_{0.5}Zr_{0.5}O₂ support particles (5–10 nm) renders a very low contrast between the structure of the metal particles and oxide support.

Nevertheless, Pd was detected after subsequent energy dispersive X-ray spectroscopy (EDS) analyses taken from more than 20 different regions of the sample with areas between 100 and 500 nm². The atomic concentration of Pd based on EDS analyses was found to be 1.9 ± 1.5 wt% (varying in the 0–4.5 wt% range), implying a wide distribution of Pd particle size in the solid sample; the number 1.9 reflects the mean value, while that of 1.5 the standard deviation. Thus, the combined information obtained through HR-TEM images and EDS analyses leads to the conclusion that Pd is extremely well dispersed on the support with an estimated mean particle size of about 1.5 nm.

The mean atom-% Ce concentration with respect to the total Ce + Zr present in the sample was estimated to be 44 ± 17 atom% (Table 3). The value of the standard deviation signifies the degree of phase segregation given the fact that the Ce/(Ce + Zr) ratio was found to range between 71 (Ce-rich phases) and 20 (Zr-rich phases) atom%. Phase heterogeneity was further studied by means of EDS linear profiles. Fig. 2c presents a HAADF-STEM image of the fresh Pd/Ce_{0.5}Zr_{0.5}O₂ sample. The intensity profiles of the Pd- $\text{L}\alpha_1$, Zr- $\text{L}\alpha_1$, and Ce- $\text{K}\alpha_1$ X-ray energy lines on the HAADF-STEM image reveal partial segregation of Ce and Zr phases. The appearance of the Pd- $\text{L}\alpha_1$ X-ray energy line confirms the presence of palladium in the sample, with Pd concentrating in Ce-rich regions, probably due to strong Pd–Ce interactions [43].

Modification of the Pd/Ce_{0.5}Zr_{0.5}O₂ catalyst by P, P–Ca and P–Zn incorporation did not alter significantly the Pd concentration except in the case of the P–Zn poisoned sample for which the Pd composition was found to be 0.8 ± 0.7 wt% (varying in the 0–2.4 wt% range, Table 3). Therefore, it might be said that deposition of Zn on the catalyst results to surface reconstruction covering Pd particles. The mean atomic Ce/Zr ratio was found to be close to 1.0 in all samples.

Fig. 3a shows a TEM image of the P–Pd/Ce_{0.5}Zr_{0.5}O₂ sample, where an amorphous layer can be seen around some of the catalyst particles. EDS analyses performed on regions where this amorphous layer was detected revealed the presence of P (indicated by arrows), while several regions were found to be uncontaminated (Fig. 3b). In the presence of Ca or Zn no isolated particles of CaO or ZnO were detected, although their presence along with Pd, Ce and Zr was confirmed by EDS. The concentration of P, Ca and Zn in the amorphous layer of contaminated samples was found to be less than 1 wt%.

3.1.4. Pd dispersion—H₂ chemisorption/TPD studies

Fig. 4 presents temperature-programmed desorption profiles of hydrogen (H₂-TPD) obtained over the Pd/Ce_{0.5}Zr_{0.5}O₂ catalysts (fresh and aged) before and after P, P–Ca and P–Zn deposition

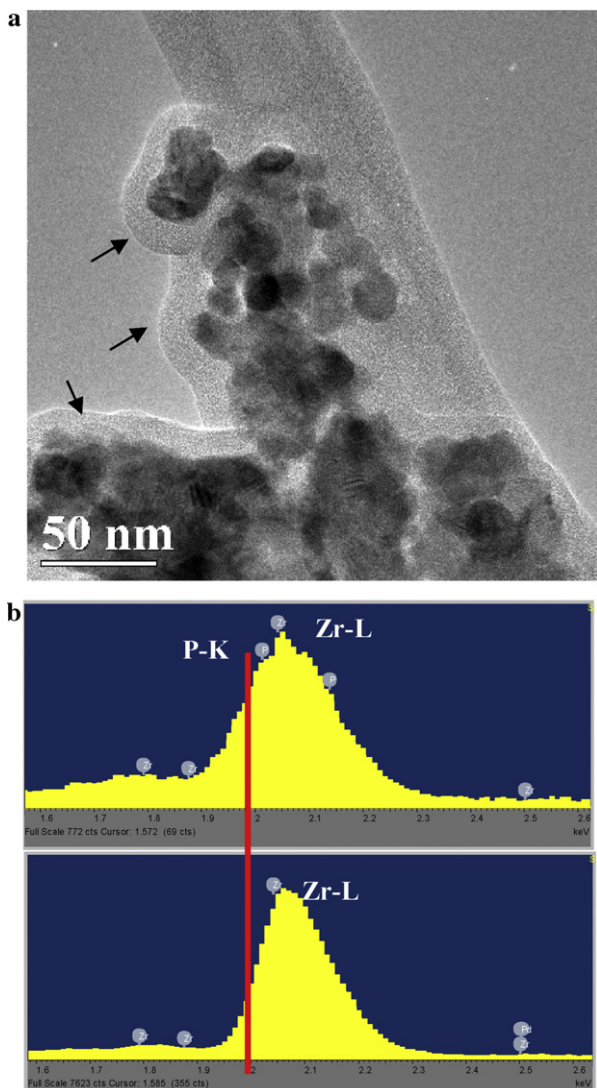


Fig. 3. (a) HAADF-STEM image of P-Pd/Ce_{0.5}Zr_{0.5}O₂ catalyst; (b) comparison between EDS spectra taken from two regions of the catalyst with and without the amorphous layer (see arrows in (a)).

(aged samples). The inset figure shows the TPD profile of the Pd/Ce_{0.5}Zr_{0.5}O₂-fresh catalyst after deconvolution, which is well described ($R^2 = 0.9992$) by four individual hydrogen desorption peaks centered at 90, 140, 235 and 340 °C (see inset, Fig. 4). In the case of the aged catalyst, a very similar TPD profile was obtained to that observed in the fresh one. During hydrogen adsorption on palladium surfaces, di-hydrogen is dissociated on the surface, and depending on the temperature and hydrogen pressure used, the hydrogen atoms interact with Pd in two states: the α -state

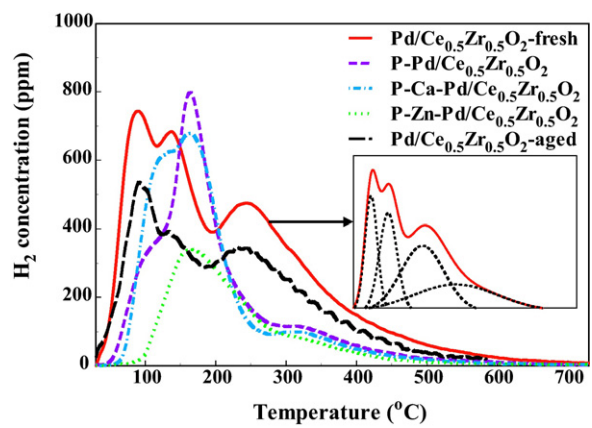


Fig. 4. H₂-TPD profiles obtained over the non-contaminated and P, P-Ca and P-Zn contaminated Pd/Ce_{0.5}Zr_{0.5}O₂ catalysts. The inset shows the deconvoluted H₂-TPD profile of Pd/Ce_{0.5}Zr_{0.5}O₂-fresh catalyst into four desorption peaks.

corresponding to dissolved hydrogen in the bulk of Pd, and the β -state corresponding to adsorbed atomic hydrogen [44]. To avoid hydrogen dissolution in the metal, and hydride formation, all the necessary precautions were taken in the experimental procedure as outlined in a previous study [34]. The appearance of the first three low-temperature desorption peaks (at 90, 140, and 235 °C, inset Fig. 4) in the Pd/Ce_{0.5}Zr_{0.5}O₂-fresh solid indicates that several adsorption states exist, which is the result of occurrence of different adsorption centers of specific bond strengths (E_{Pd-H} , kcal/mol) for hydrogen [44,45]. The high-temperature small desorption peak centered at 340 °C is likely to be associated with H₂ desorption due to some hydrogen spillover from the metal onto the support that took place during the adsorption step, promoting, therefore, some surface reduction of the Ce_{0.5}Zr_{0.5}O₂ mixed metal oxide [46]. Aging of the catalyst at 850 °C appears not to result in any shift in the position of all desorption peaks, while it only causes some reduction in their intensity. The latter reflects sintering effects due to the increase of calcination temperature, thus some loss of Pd adsorption sites.

The addition of phosphorous onto the Ce_{0.5}Zr_{0.5}O₂-supported Pd catalyst causes a considerable shift towards higher desorption temperatures (Fig. 4). In particular, the first low-temperature desorption peak attributed to adsorption of hydrogen on surface Pd atoms was not only shifted from 90 to 120 °C (Fig. 4) when P was added, but also decreased substantially in size, which reflects the decrease in the amount of hydrogen adsorbed (Table 3). In the case where Ca was also present together with P, the corresponding desorption peak area increased slightly, while in the presence of Zn-P this peak had disappeared. The second desorption peak corresponding to the Pd/Ce_{0.5}Zr_{0.5}O₂-fresh catalyst and located at 140 °C was also shifted to higher temperatures (160 °C), and significantly reduced in size after adding P and Zn. These results strongly suggest that the presence of P, Ca or Zn contaminants strongly affects the

Table 3
H₂ adsorption ($\mu\text{mol H/g}_{\text{cat}}$), metal dispersion (D, %), mean Pd particle size (d_{Pd} , nm), Pd concentration (wt%), and %Ce atom ratio ($\text{Ce}/(\text{Ce} + \text{Zr}) \times 100$) estimated for the non-contaminated and contaminated with P, P-Ca or P-Zn Pd/Ce_{0.5}Zr_{0.5}O₂ solids based on H₂-TPD and HRTEM measurements.

Catalyst	H ₂ adsorption ($\mu\text{mol H/g}_{\text{cat}}$)	D (%)	d_{Pd} (nm)	Pd (wt%) \pm s.d.	%Ce \pm s.d. ^a
Pd/Ce _{0.5} Zr _{0.5} O ₂ -fresh	68.6	73.0	1.5	1.9 \pm 1.5	44 \pm 17
Pd/Ce _{0.5} Zr _{0.5} O ₂ -aged ^b	59.3	63.1	1.7	–	–
P-Pd/Ce _{0.5} Zr _{0.5} O ₂ -aged	51.0	–	–	1.7 \pm 1.9	47 \pm 16
P-Ca-Pd/Ce _{0.5} Zr _{0.5} O ₂ -aged	55.3	–	–	1.9 \pm 1.8	46 \pm 5
P-Zn-Pd/Ce _{0.5} Zr _{0.5} O ₂ -aged	20.9	–	–	0.8 \pm 0.7	48 \pm 6

^a %Ce = Ce/(Ce + Zr) $\times 100$.

^b Calcination in air at 850 °C for 4 h (Section 2.1).

desorption kinetics of H_2 associated with the Pd surface. A similar behaviour was observed after Fe deposition on Pd-Rh/CeO₂-Al₂O₃ catalyst [47], where the electronic environment of the Pd surface atoms was found to change due to the presence of Fe, thus affecting their chemisorptive properties. On the other hand, XPS analysis (Section 3.2) shows that the Pd oxidation state was not affected by the deposition of contaminants. Thus, it can be suggested that the extent of hydrogen adsorption and desorption kinetics on palladium is influenced by the formation of new phases that originate from P, Ca or Zn inhibitors that partially cover a number of Pd particles.

Based on the amount of hydrogen desorbed up to 300 °C [46], the dispersion (D , %) of Pd was estimated for the fresh and aged Pd/Ce_{0.5}Zr_{0.5}O₂ catalysts, and this is reported in Table 3. It is noted that the theoretical amount of surface hydrogen estimated, based on the assumption of a unity adsorption stoichiometry ($H/Pd_s = 1.0$) and $D = 100\%$, is 94.0 μmol H per gram of catalyst (μmol H/g_{cat}) considering a Pd metal loading of 1.0 wt%. By comparing the amounts of H species chemisorbed (Table 3), it is clearly seen that in all cases the value of H/Pd_T is lower than 1.0; Pd_T is the total number of Pd (μmol) in the sample. The average Pd particle size (d_{Pd} , nm) in the Pd/Ce_{0.5}Zr_{0.5}O₂-fresh catalyst was estimated using the relationship d (nm) = $1.13/D \times 100$ [49], and this was found to be 1.5 nm. The d_{Pd} was found to increase to 1.7 nm after calcination (aged sample), which implies sintering of the Pd particles by increasing the calcination temperature from 500 to 850 °C. It appears that the accumulation of phosphorus on the catalyst surface leads to significant reduction (~25%) of Pd metal surface sites, and this reduction is largely due to the presence of contaminants, as evidenced by the TEM and EDS measurements, and only slightly to the agglomeration of Pd particles. Zn addition further enhanced the negative effect of P deposition due to the formation of new phases on the catalyst surface (e.g., CePO₄, XRD), and ZnO (XPS, Section 3.2).

3.2. Surface redox properties of non-contaminated and contaminated with P, P-Ca and P-Zn Pd/Ce_{0.5}Zr_{0.5}O₂ catalysts

The effects of poisoning by P, Ca and Zn of the model Pd/Ce_{0.5}Zr_{0.5}O₂ “three-way” catalyst on its surface redox properties were investigated by the use of XPS. The sample was first treated in 20 vol% O₂/Ar at 500 °C for 2 h, and then reduced in pure hydrogen at 300 °C for 2 h. Table 4 reports the binding energies (BE, eV) of Pd 3d_{5/2}, Ce 3d_{5/2}, Zr 3d_{5/2}, O 1s, P 2p, Ca 2p_{3/2} and Zn 2p_{3/2} core levels of the Pd/Ce_{0.5}Zr_{0.5}O₂ samples after oxidation.

Fig. 5 presents Pd 3d photoelectron spectra recorded over the Pd/Ce_{0.5}Zr_{0.5}O₂-fresh catalyst after reduction in H₂ (Fig. 5a) and after subsequent exposure to 20 vol% O₂/He gas mixture (Fig. 5b). After H₂ reduction, the Pd 3d_{5/2} and 3d_{3/2} peaks (Fig. 5a) appear at 335.3 and 341.5 eV, respectively, due to reduction of Pd²⁺ to metallic Pd⁰. After oxidation, the Pd 3d_{5/2} and 3d_{3/2} peaks (Fig. 5b) were shifted to higher BE at about 337.1 and 342.4 eV, respectively, which correspond to Pd²⁺ (palladium oxide, PdO) [50]. These results indicate that Pd was fully reduced and oxidised at the applied oxidative and reductive treatment conditions. Deposition of contaminants on the catalyst surface was found not to influence palladium redox state since the positioning of the Pd XP peaks was found not to be affected (see BE of Pd 3d_{5/2}, Table 4). The latter demonstrates that the presence of P alone or in combination with Ca or Zn appears not to affect the local electronic environment of Pd metal surface atoms.

The P 2p_{3/2} core level peak was found to be located at 133.3 ± 0.1 eV (Table 4). This position is attributed to P-O bonds in PO₄³⁻ chemical environment, like in CePO₄ [51]. Moreover, the BE of Ca 2p_{3/2} electrons at 347.7 eV is in harmony with that reported for calcium phosphate salts, such as Ca₃(PO₄)₂, while it is far from that of 346.1 eV measured over CaO [50,52]. On the

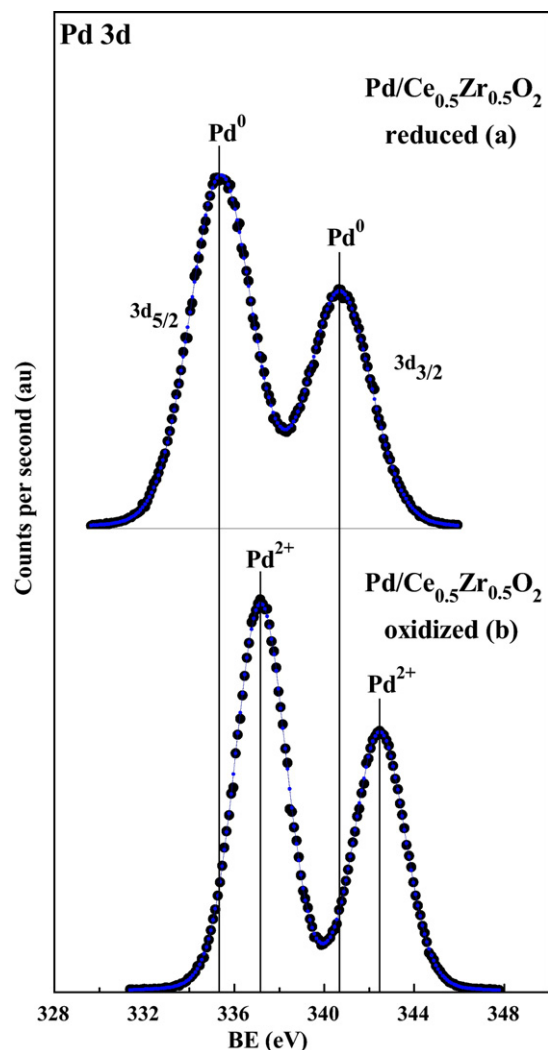


Fig. 5. X-ray photoelectron spectra of Pd 3d core level obtained over the (a) reduced (H_2 , 1 bar, 300 °C, 2 h) and (b) oxidised (20 vol% O₂/Ar, 500 °C, 2 h) Pd/Ce_{0.5}Zr_{0.5}O₂-fresh catalyst.

other hand, in the case of zinc, the Zn 2p_{3/2} located at 1022.0 eV in the P-Zn/Ce_{0.5}Zr_{0.5}O₂ sample is typical of zinc(II) oxide (ZnO) and not of Zn₃(PO₄)₂ for which the respective value is 1024.7 eV [50]. This remark is strengthened by the fact that the major O 1s peak component obtained for the O 1s core-level at 529.9 eV (Table 4) corresponds to that measured over ZnO [50]. These results imply that Zn deposition resulted in highly dispersed particles of ZnO on the catalyst surface. In the case of the non-contaminated Pd/Ce_{0.5}Zr_{0.5}O₂ solid, the major O 1s component observed at 529.6 eV and assigned to surface lattice oxygen, O²⁻, and the additional component at 531.2 eV due to adsorbed oxygen species, such as O⁻, O₂²⁻ or O₂⁻, are in accordance to those measured over the CeO₂-ZrO₂ solid solution [53]. For P and P-Ca contaminated samples the binding energy of the O 1s peak was found to be shifted to higher values by 0.4–0.6 eV with respect to the value obtained for the non-contaminated Pd/Ce_{0.5}Zr_{0.5}O₂ solid (Table 4). This shift is due to the presence of Ce–O–P bonds and the Ce(III) oxidation state [51].

Fig. 6 presents X-ray photoelectron spectra of the Ce 3d core-level for the non-contaminated Pd/Ce_{0.5}Zr_{0.5}O₂ catalyst after reduction (Fig. 6a), and after oxidation (Fig. 6b). According to the thoroughly accepted convention suggested by Burroughs et al. [54], Ce3d_{3/2} multiplets are labelled ν , whereas those of 3d_{5/2} are

Table 4

Binding energies (eV) of core levels estimated for the non-contaminated and contaminated with P, P-Ca and P-Zn Pd/Ce_{0.5}Zr_{0.5}O₂ aged^a catalysts after oxidation (20 vol%O₂/Ar, 500 °C, 2 h) in the XPS instrument.

Supported Pd catalyst	Pd 3d _{5/2}	Ce 3d _{5/2}	Zr 3d _{5/2}	P 2p	Ca 2p _{3/2}	Zn 2p _{3/2}	O 1s
Pd/Ce _{0.5} Zr _{0.5} O ₂	337.2	882.4	182.2	–	–	–	529.6
P-Pd/Ce _{0.5} Zr _{0.5} O ₂	337.1	882.6	182.2	133.3	–	–	531.2
P-Ca-Pd/Ce _{0.5} Zr _{0.5} O ₂	337.2	882.7	182.1	133.2	347.7	–	530.0
P-Zn-Pd/Ce _{0.5} Zr _{0.5} O ₂	337.1	882.7	182.2	133.4	–	1022.0	531.6
							531.8
							530.2
							529.9
							531.4

^a Calcination in air at 850 °C for 4 h (Section 2.1).

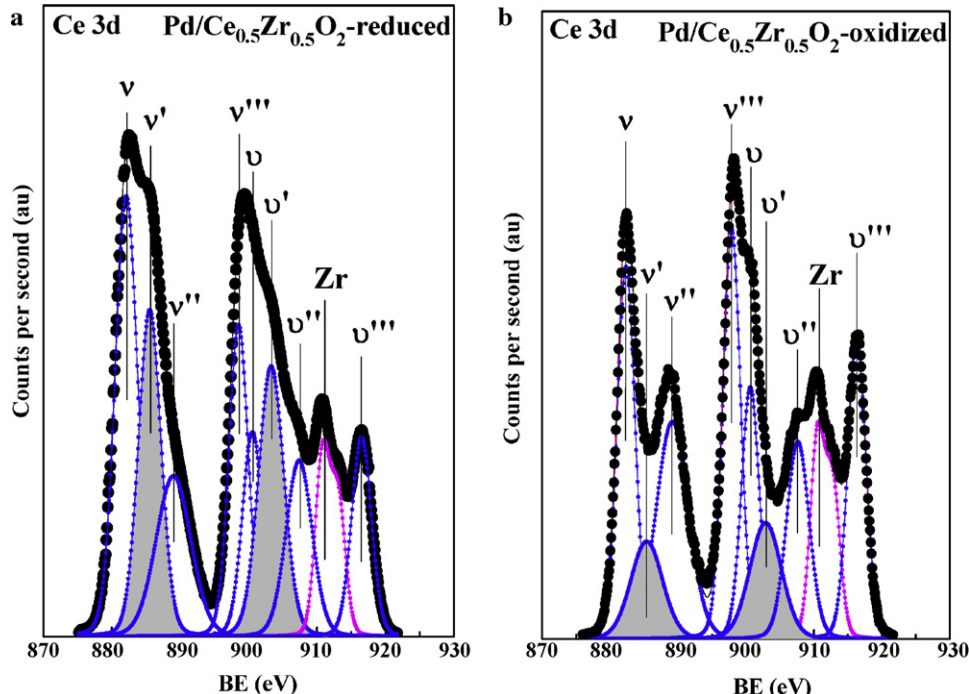


Fig. 6. X-ray photoelectron spectra of Ce 3d core level obtained over Pd/Ce_{0.5}Zr_{0.5}O₂-fresh catalyst after (a) reduction (H₂, 1 bar, 300 °C, 2 h) and (b) oxidation (20 vol%O₂/Ar, 500 °C, 2 h).

labelled ν . In the XP spectrum of pure Ce(IV) oxide, ν , ν'' and ν''' peaks can be observed for the Ce3d_{5/2} core level, and ν , ν'' and ν''' peaks for the Ce3d_{3/2} level, while for pure Ce(III) oxide, ν' and ν' features can be seen [54]. As seen in Fig. 6, both Ce(IV) and Ce(III) features coexist in the XP spectra of the Pd/Ce_{0.5}Zr_{0.5}O₂ solid. This means that after its exposure to oxidising conditions, Ce⁴⁺ is populated at least in the surface region of the powder particles, while a small fraction of Ce still remains as Ce³⁺ species (ν' and ν' shaded peaks in Fig. 6b). Based on this information, a quantitative estimation of the degree of reduction of Ce(IV) oxide can be made by calculating the percent fraction of the Ce⁴⁺ species on the sample surface as previously described [30], where the integral areas of the Ce³⁺ and Ce⁴⁺ XP peaks (after fitting) were used. In a recent work [55], the area under the Ce³⁺/Ce⁴⁺ XP peaks was estimated by the product: FWHM \times I, where FWHM is the full width of the peak at half maximum, and I is the height of the peak.

The % Ce⁴⁺ values calculated over the non-contaminated and contaminated Pd/Ce_{0.5}Zr_{0.5}O₂ samples are given in Table 5. In the absence of contaminants, the Pd/Ce_{0.5}Zr_{0.5}O₂ solid displayed the highest percentage of Ce⁴⁺ (84%) after oxidation, while the percent fraction of Ce⁴⁺ species in the contaminated by P, P-Ca and P-Zn catalysts is reduced to ~66%. This means that a large fraction of Ce³⁺ species exists on the surface of the phosphated Pd/Ce_{0.5}Zr_{0.5}O₂

solids that is difficult to be re-oxidised into Ce⁴⁺ even after calcination (20% O₂/He gas flow) in the 500–850 °C range due to the formation of highly stable CePO₄ [12,24]. We have previously reported [30] that the surface %Ce⁴⁺ on the same support material after being contaminated with the same loading of P, Ca or Zn and subjected to the same aging conditions (air, 850 °C, 4 h) presented significantly lower values. For example, in the case of P and P-Zn, the %Ce⁴⁺ was 46.0 and 37.0, respectively, to be compared to 66% found in the present case of supported-Pd solid. This is a very important result pointing out the positive effect of Pd in preventing the deactivation of the OSC property (Ce³⁺ is mainly associated

Table 5

XPS surface atom ratios and %Ce⁴⁺ estimated for the non-contaminated and contaminated with P, P-Ca and P-Zn Pd/Ce_{0.5}Zr_{0.5}O₂ aged^a catalysts after oxidation (20 vol%O₂/Ar, 500 °C, 2 h) in the XPS instrument.

Supported Pd catalyst	Pd/Zr	Ce/Zr	P/Zr	Ca/Zr	Zn/Zr	%Ce ⁴⁺
Pd/Ce _{0.5} Zr _{0.5} O ₂ -fresh	0.080	1.277	–	–	–	84
P-Pd/Ce _{0.5} Zr _{0.5} O ₂	0.054	0.987	0.494	–	–	66
P-Ca-Pd/Ce _{0.5} Zr _{0.5} O ₂	0.058	1.166	0.617	0.250	–	67
P-Zn-Pd/Ce _{0.5} Zr _{0.5} O ₂	0.065	0.959	0.488	–	0.251	66

^a Calcination in air at 850 °C for 4 h (Section 2.1).

with the formation of CePO_4), which is indeed confirmed by OSC measurements (Section 3.3).

Table 5 also reports the surface atom ratios of Pd/Zr, Ce/Zr, P/Zr, Ca/Zr and Zn/Zr estimated for the Pd/ $\text{Ce}_{0.5}\text{Zr}_{0.5}\text{O}_2$ solids via the XPS studies. The Pd/Zr atom ratio is found to decrease by 20–33% after deposition of contaminants, which is most likely due to the coverage of a large number of Pd particles by contaminants compounds. Small variations in the Pd/Al surface atom ratio between the contaminated samples could be due to some overlapping with the $\text{Zr} 3\text{p}_{3/2}$ XP peak. The surface of the non-contaminated Pd/ $\text{Ce}_{0.5}\text{Zr}_{0.5}\text{O}_2$ catalyst is found to be enriched with cerium to a small extent, since the experimental Ce/Zr surface ratio of 1.277 obtained is slightly higher than the nominal one (Ce/Zr = 1.0), which is in agreement with the EDS profile analysis performed. After P and P-Zn poisoning, the Ce/Zr ratio is found to decrease by ~25%, whereas in the presence of Ca surface rearrangement of Ce and Zr atoms appears to be hindered due to the participation of at least a fraction of P towards the formation of $\text{Ca}_3(\text{PO}_4)_2$. The latter hinders P from reacting with Ce and reconstructing the catalyst surface. Based on the amounts used in the catalyst's preparation stage, and in the case where P, Ca and Zn elements would have been uniformly distributed within the lattice of the $\text{Ce}_{0.5}\text{Zr}_{0.5}\text{O}_2$ solid solution, the nominal values of P/Zr, Ca/Zr and Zn/Zr “bulk” atom ratios would be equal to 0.428, 0.074 and 0.045, respectively. It is noticed that the Ca/Zr and Zn/Zr surface atom ratios (~0.250, Table 5) are considerably higher than the “bulk” ones, illustrating that Ca and Zn poisons are highly concentrated on the surface of the Pd/ $\text{Ce}_{0.5}\text{Zr}_{0.5}\text{O}_2$ solid. In particular, Ca and Zn surface ratios with respect to Zr were found to be larger than the respective bulk values by a factor of 3.4 and 5.6, respectively, demonstrating that Ca^{2+} and Zn^{2+} ions have not been incorporated within the framework of $\text{Ce}_{0.5}\text{Zr}_{0.5}\text{O}_2$ but instead they were highly dispersed on the catalyst surface as small amorphous particles of $\text{Ca}_3(\text{PO}_4)_2$ and ZnO , as already discussed.

On the contrary, the value of surface P/Zr atom ratio estimated over the contaminated samples is very close to the “bulk” value, which implies that phosphorus (in the form of PO_4^{3-}) is incorporated within the solid framework, at least in the upper few monolayers beyond the surface layer. Larese et al. [24] deliberately deposited phosphorus on CeO_2 and $\text{Ce}_x\text{Zr}_{1-x}\text{O}_2$ solid solution and proposed, based on spectroscopic experimental evidence, that CePO_4 predominates at the surface/subsurface of the resulting material upon reaction of the incorporated P with the Ce(-Zr) oxides. Moreover, based on the P, Ca and Zn amounts added during the present catalysts synthesis, the number of P, Ca and Zn atoms added with respect to the number of surface oxygen atoms can be evaluated, taking into account that for $\text{Ce}_{0.5}\text{Zr}_{0.5}\text{O}_2$ there are 13.7 superficial oxygen atoms per nm^2 of the solid surface [56]. $\text{P}/\text{O}_{\text{surf}}$, $\text{Ca}/\text{O}_{\text{surf}}$ and $\text{Zn}/\text{O}_{\text{surf}}$ can be used as an estimate of catalyst surface coverage in P, Ca and Zn, respectively, based on the amounts added. When this ratio is equal to 1.0, then it might be said that the surface can be fully covered by contaminants, and that an atomic monolayer of contaminants atoms is theoretically formed on the surface of the solid. The results from these calculations are as follows: $\text{P}/\text{O}_{\text{surf}} = 1.261$, $\text{Ca}/\text{O}_{\text{surf}} = 0.216$, and $\text{Zn}/\text{O}_{\text{surf}} = 0.133$, which show that the contaminants number density used exceeds that of a surface monolayer.

The highest P/Zr surface atom ratio was measured over the P-Ca-Pd/ $\text{Ce}_{0.5}\text{Zr}_{0.5}\text{O}_2$ sample. This proves that the addition of Ca with P prevents a fraction of P from migrating deeply into the subsurface layers of the solid, most likely due to the formation of $\text{Ca}_3(\text{PO}_4)_2$. In earlier studies it was shown that the presence of Ca in lubricants can lead to the formation of powdery phosphate salts on a TWC surface [40]. On the contrary, Zn addition was found not to inhibit P penetration within the catalyst washcoat layer, probably because

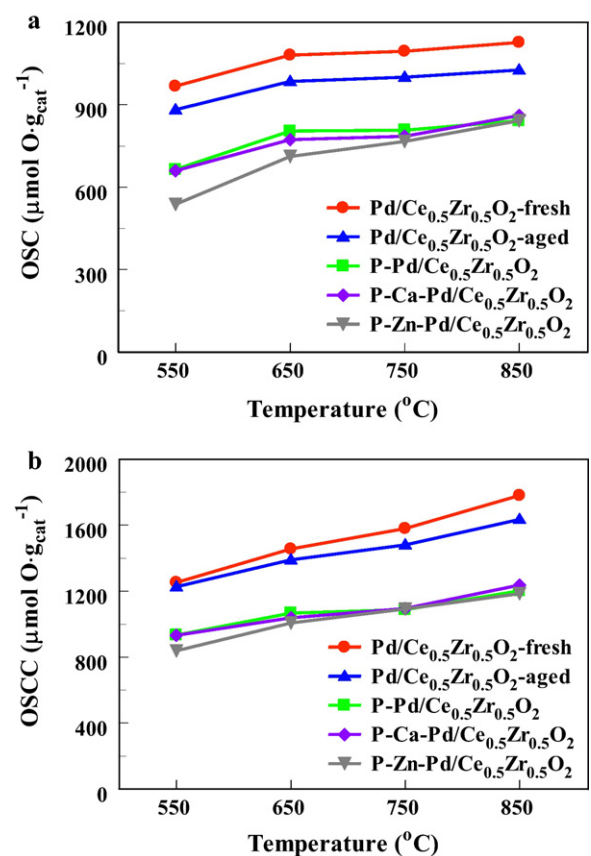


Fig. 7. OSC (a) and OSCC (b) quantities ($\mu\text{mol O/g}$) measured over the fresh and aged non-contaminated, and P, P-Ca and P-Zn contaminated Pd/ $\text{Ce}_{0.5}\text{Zr}_{0.5}\text{O}_2$ catalysts in the 550–850 °C range.

zinc exists in the form of ZnO particles, and not as $\text{Zn}_3(\text{PO}_4)_2$, thus favouring the reaction of PO_4^{3-} with Ce to form CePO_4 .

3.3. Oxygen storage and release properties of non-contaminated and contaminated with P, P-Ca and P-Zn Pd/ $\text{Ce}_{0.5}\text{Zr}_{0.5}\text{O}_2$ catalysts

Fig. 7 presents OSC (Fig. 7a) and OSCC (Fig. 7b) quantities ($\mu\text{mol O/g}_{\text{cat}}$) measured over the fresh, aged, and contaminated with P, P-Ca and P-Zn Pd/ $\text{Ce}_{0.5}\text{Zr}_{0.5}\text{O}_2$ model “three-way” catalysts in the 550–850 °C range. It should be remarked here that prior to injecting the H_2 pulse(s), the Pd and $\text{Ce}_{0.5}\text{Zr}_{0.5}\text{O}_2$ particles are completely oxidised [34,48]. During OSC and OSCC measurements, the following key steps might have taken place successively [57,58]: (i) reduction of PdO by hydrogen to produce water and metallic Pd^0 , (ii) hydrogen dissociative chemisorption on Pd, and formation of PdH_x hydride (reversible step), (iii) hydrogen spillover from the metal to the $\text{Ce}_{0.5}\text{Zr}_{0.5}\text{O}_2$ support, (iv) oxygen back-spillover from the surface of $\text{Ce}_{0.5}\text{Zr}_{0.5}\text{O}_2$ support to the Pd^0 phase, (v) surface reduction of $\text{Ce}_{0.5}\text{Zr}_{0.5}\text{O}_2$ with the formation of anionic vacancies, and (v) oxygen diffusion from the bulk of $\text{Ce}_{0.5}\text{Zr}_{0.5}\text{O}_2$ to the surface, and hence bulk reduction. As illustrated in Fig. 7, a remarkable drop in the OSC (Fig. 7a) and OSCC (Fig. 7b) occurs in the entire temperature range investigated, after contamination of Pd/ $\text{Ce}_{0.5}\text{Zr}_{0.5}\text{O}_2$ with P, P-Ca and P-Zn. This means that incorporation of these poisons in the Pd/ $\text{Ce}_{0.5}\text{Zr}_{0.5}\text{O}_2$ catalyst has negatively influenced its ability to store and release oxygen from its surface and subsurface/bulk structure. These poisons either act as inhibitors of surface and bulk oxygen diffusion or alter the oxygen chemisorptive properties of $\text{Ce}_{0.5}\text{Zr}_{0.5}\text{O}_2$ solid surface, which all are associated with the oxygen storage and

release processes. The OSC and OSCC quantities measured in the 550–850 °C range over the contaminated supported-Pd catalysts were found to decrease by ~170–450 $\mu\text{mol O g}_{\text{cat}}^{-1}$ with respect to the Pd/Ce_{0.5}Zr_{0.5}O₂-aged solid, which in terms of percentage reduction in oxygen storage capacity is between 16 and 40%. The most significant decrease in the OSC of Pd/Ce_{0.5}Zr_{0.5}O₂ was observed at the lowest reaction temperature of 550 °C (Fig. 7a). In particular, the non-contaminated aged catalyst presents the highest OSC (882 $\mu\text{mol O g}_{\text{cat}}^{-1}$), while this value is reduced by ~25% when P or P-Ca is added. In the presence of P-Zn, OSC reduction is even more pronounced reaching the value of ~40%. As far as the OSCC measured at 550 °C (Fig. 7b), about 23–32% reduction is observed. Similar results were also obtained at higher reaction temperatures (16–28% reduction in OSC and OSCC). The number of oxygen monolayers involved in the storage/release processes was calculated on the basis of the experimental OSC and OSCC values and the theoretical number density of surface oxygen atoms, namely, 13.7 atoms nm^{−2} for the Ce_{0.5}Zr_{0.5}O₂ solid [56]. At low reaction temperatures ($T \leq 550$ °C), the OSC mostly reflects surface labile oxygen present in the PdO phase and the surface of ceria-zirconia solid support; the number of oxygen monolayers was estimated to be equal or lower than one under the experimental conditions applied for the OSC measurement. Bedrane et al. [58] showed that the activation of oxygen on ceria or ceria-zirconia supported catalysts is fast, with metal particles acting as portholes for the subsequent migration and storage of oxygen on the support. Thus, at low reaction temperatures, palladium dispersion would play a very important role since the transient rates of H₂ oxidation on PdO and that of the back-spillover of oxygen from the mixed oxide to the Pd/PdO interface were found to decrease by increasing the Pd particle size [48]. This was ascribed to the weakening of the metal-support interactions which are crucial for promoting oxygen mobility and reactivity [48,58]. In the present study, the Pd particles were found to be partly covered by P, Ca and/or Zn compounds formed after deliberately poisoning the catalyst. As a result, a significant deterioration of the oxygen storage and release properties of the Pd/Ce_{0.5}Zr_{0.5}O₂ solid was observed. The lowest Pd surface sites per gram of catalyst and BET surface area measured over the P-Zn-Pd/Ce_{0.5}Zr_{0.5}O₂ catalytic system must be related to the inhibition of steps (i)–(iv) mentioned above, and these are in accordance with the lowest OSC (Fig. 7a) and OSCC (Fig. 7b) values measured at 550 °C.

In previous studies [25–27], although the deterioration of the oxygen storage and release properties of CeO₂ and Ce_xZr_{1-x}O₂ materials by phosphorus addition was investigated thoroughly, those studies were performed on the support materials alone, in the absence of a noble metal. In order to emphasize the important role the Pd metal plays on the OSC process, it should be mentioned that OSC measurements conducted in the absence of Pd over the non-contaminated and contaminated with P, P-Ca and P-Zn Ce_{0.5}Zr_{0.5}O₂ solids [30] were found to be up to 10 times lower compared to those found in the respective supported-Pd catalysts measured in the present work. Also, the % reduction in OSC and OSCC at 550 °C after poisoning the Ce_{0.5}Zr_{0.5}O₂ support was found to be about 50–70% [30] compared to 16–40% found for the respective Pd/Ce_{0.5}Zr_{0.5}O₂ solids. More precisely, the OSC values measured over the Pd/Ce_{0.5}Zr_{0.5}O₂-aged solid is four times larger than in the case of Ce_{0.5}Zr_{0.5}O₂-aged alone (882 vs. 223 $\mu\text{mol O g}^{-1}$, $T = 550$ °C). After deposition of P, Ca and/or Zn contaminants on the Ce_{0.5}Zr_{0.5}O₂ and Pd/Ce_{0.5}Zr_{0.5}O₂ solids, even though the OSC and OSCC values were significantly lower compared to the non-contaminated ones, these were found to be by 7–10 times higher on the contaminated Pd/Ce_{0.5}Zr_{0.5}O₂ solids compared to the respective contaminated Ce_{0.5}Zr_{0.5}O₂ solids. For example, the OSC of P/Ce_{0.5}Zr_{0.5}O₂ is 68 $\mu\text{mol O g}^{-1}$ and that of P-Pd/Ce_{0.5}Zr_{0.5}O₂ is 665 $\mu\text{mol O g}^{-1}$ at 550 °C. As the

reaction temperature increases, the differences between the poisoned Ce_{0.5}Zr_{0.5}O₂ and Pd/Ce_{0.5}Zr_{0.5}O₂ solids become less pronounced.

Based on the above offered discussion, it can be stated that the presence of Pd on the surface of Ce_xZr_{1-x}O₂ support material reduces to a considerable degree the negative effects of P, Ca and Zn imposed on their oxygen storage and release properties, most likely through the promotion of hydrogen and oxygen dissociation and activation steps (i)–(iii), and that of the back-spillover of oxygen from Ce_{0.5}Zr_{0.5}O₂ to the oxygen vacant sites of surface Pd in its reduced state (step (iv)) [48]. At reaction temperatures higher than 550 °C, surface reduction of Ce_{0.5}Zr_{0.5}O₂ (step (v)) and oxygen diffusion from the bulk of Ce_{0.5}Zr_{0.5}O₂ particles take place, supplying oxygen on the surface (step (vi)). However, as seen in Fig. 7, OSC and OSCC quantities at $T > 650$ °C are drastically suppressed after P, P-Ca and P-Zn deposition on the Pd/Ce_{0.5}Zr_{0.5}O₂ catalyst. It is also worth pointing out that calcination of the latter solid at 850 °C for 4 h (aged sample) only slightly affected the OSC (up to 10% reduction), whereas the OSCC was not affected. This is due to some reduction in the BET surface area upon aging, which results in a small reduction in the concentration of labile surface oxygen species. The present results (Fig. 7) indicate that the presence of P, P-Ca or P-Zn contaminants on the catalyst surface largely reduces the concentration of labile oxygen species in the catalyst. This is due to the formation of amorphous phosphate layer of CePO₄ and/or Ca₃(PO₄)₂ that physically covers and binds catalyst's surface Oⁿ⁻ species, thus suppressing the rates of surface and bulk oxygen diffusion.

3.4. Catalytic performance of non-contaminated and contaminated with P, P-Ca and P-Zn Pd/Ce_{0.5}Zr_{0.5}O₂ solids

In order to investigate the effects of chemical poisoning of Pd/Ce_{0.5}Zr_{0.5}O₂ solid on its catalytic performance, probe reactions related to the TWC chemistry, namely CO and C₃H₆ oxidation and NO reduction by H₂ were examined. It should be noted that the used feed concentrations of CO, C₃H₆, NO, H₂ and O₂ were representative average values found in the exhaust gas stream at the inlet of a “three-way” catalyst installed in a gasoline-driven car.

Fig. 8 presents TPSR profiles for (a) CO and C₃H₆ conversion (1%CO/0.2%C₃H₆/1%O₂/He) obtained over the non-contaminated Pd/Ce_{0.5}Zr_{0.5}O₂-aged catalyst, and (b) CO conversion profile obtained over the non-contaminated-aged and contaminated with P, P-Ca and P-Zn Pd/Ce_{0.5}Zr_{0.5}O₂-aged catalysts. At reaction temperatures around 200 °C, under the lean-oxygen conditions employed, CO is completely converted into CO₂ over the non-contaminated supported Pd catalyst, while C₃H₆ conversion is only partial ($X_{\text{C}_3\text{H}_6} < 35\%$). This result indicates that Pd/Ce_{0.5}Zr_{0.5}O₂ is more active towards CO than C₃H₆ oxidation at low reaction temperatures when both are present in the exhaust gas stream. At $T > 300$ °C, oxygen was found to be totally consumed by the catalyst ($X_{\text{O}_2} = 100\%$), while at the same time, as seen in Fig. 8, the CO oxidation activity of the catalyst under rich feed conditions (oxygen deficient) gradually decreases. On the other hand, C₃H₆ conversion increases and reaches the value of $X_{\text{C}_3\text{H}_6} = 100\%$ at about 450 °C, where the corresponding X_{CO} is only 55%. It is well known that the chemisorption and oxidation of propylene competes with that of CO, the latter inhibiting hydrocarbon oxidation under the stoichiometric reaction conditions TWCs operate. At low reaction temperatures, the CO coverage on Pd surface sites is high and CO is completely converted. When enough Pd sites are available at higher temperatures for the adsorption of propylene, hydrocarbon oxidation can proceed consuming most of the reactive oxygen species (C₃H₆:O₂ = 1:4.5 in the reaction C₃H₆ + 9/2O₂ → 3CO₂ + 3H₂O) and hence hindering CO oxidation [29,59,60]. Similar results were also observed in previous studies [29,59] under different feed gas

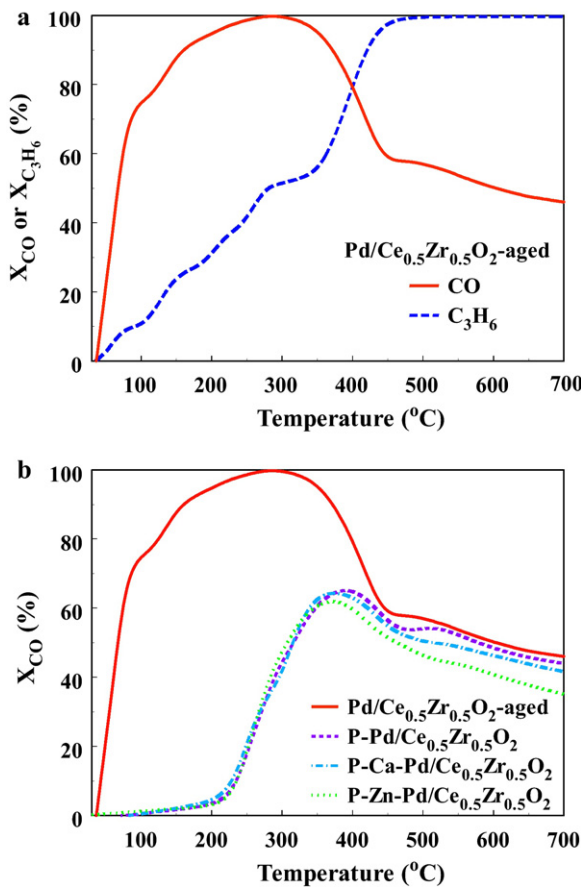


Fig. 8. TPSR profiles of CO and C₃H₆ conversions obtained over (a) Pd/Ce_{0.5}Zr_{0.5}O₂-aged catalyst and (b) P, P-Ca and P-Zn contaminated Pd/Ce_{0.5}Zr_{0.5}O₂-aged catalysts in the 30–700 °C range during CO/C₃H₆/O₂/He reaction.

compositions, and this was ascribed to the dominant capability of Pd-based catalysts towards C₃H₆ oxidation, as well as to the dynamic function of OSC by the presence of Ce_xZr_{1-x}O₂ at high temperatures.

The reaction selectivity of the non-contaminated Pd catalyst towards the CO/O₂ versus the C₃H₆/O₂ reaction in the low-temperature range of 30–300 °C was found to become less pronounced with catalyst poisoning (compare Fig. 8a and b), apparently because CO oxidation activity over the Pd-based catalyst is more severely influenced by the presence of P, Ca or Zn. This is in agreement to similar observations reported by Baik et al. [59]. As seen in Fig. 8b, X_{CO} for the contaminated samples increases with increasing reaction temperature up to ~400 °C (X_{CO} = 65%), and then decreases slightly up to 700 °C. The same behaviour was also observed by Larese et al. [24] over vehicle-aged commercial TWCs. Moreover, the CO conversion profiles of the P, P-Ca and P-Zn contaminated Pd/Ce_{0.5}Zr_{0.5}O₂ samples were found to be significantly shifted to higher temperatures compared to that of the non-contaminated Pd/Ce_{0.5}Zr_{0.5}O₂ solid. In particular, the CO conversion obtained over the non-contaminated Pd/Ce_{0.5}Zr_{0.5}O₂ reaches the value of 95% at 200 °C (T₉₅) due to the high intrinsic oxidation activity of Pd, while the activity of the contaminated ones barely starts at the same temperature (X_{CO} < 5%). Furthermore, the light-off temperature, T₅₀ (at which conversion reaches the value of 50%) is equal to 50 °C in the case of non-contaminated Pd/Ce_{0.5}Zr_{0.5}O₂ catalyst, whereas in the case of contaminated ones it is considerably higher, approximately 300 °C. It is thus obvious that deposition of P, Ca or Zn contaminants on the surface of Pd/Ce_{0.5}Zr_{0.5}O₂ solid causes a substantial increase in the T₅₀, where

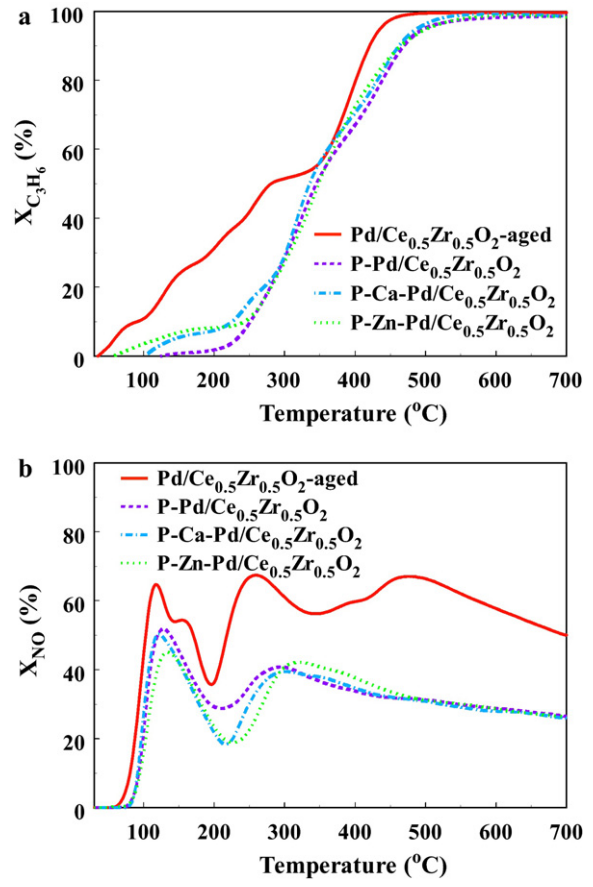


Fig. 9. (a) TPSR profiles of C₃H₆ conversion obtained during CO/C₃H₆/O₂/He reaction, and (b) TPSR profiles of NO conversion obtained during NO/H₂/O₂/He reaction over the non-contaminated and P, P-Ca and P-Zn contaminated Pd/Ce_{0.5}Zr_{0.5}O₂-aged catalysts in the 30–700 °C range.

clearly these elements act as poisons of its catalytic activity towards CO oxidation. It is also apparent from the results of Fig. 8b that no appreciable differences between the CO conversion profiles of the contaminated samples were seen, especially at T < 400 °C.

In the case of propylene oxidation reaction (Fig. 9a), the catalytic behaviour (X_{C3H6} vs. T) of the P-, P-Ca-, and P-Zn-Pd/Ce_{0.5}Zr_{0.5}O₂ catalysts were also found to be quite similar to each other, while small differences were only seen below 250 °C. Below this temperature, where CO oxidation hardly occurs on the surface of the contaminated samples (Fig. 8b), it is apparent that C₃H₆ oxidation is favoured to a small extent on the expense of CO/O₂ reaction. Moreover, the presence of P causes a pronounced decrease in propylene conversion at T < 300 °C. On the other hand, above 400 °C no appreciable discrepancies in the profiles of the contaminated and non-contaminated Pd/Ce_{0.5}Zr_{0.5}O₂ catalysts are observed. The most significant differences between the fresh and contaminated with P, P-Ca or P-Zn Pd/Ce_{0.5}Zr_{0.5}O₂ samples were noticed in the 30–340 °C and 400–500 °C temperature ranges, where Pd/Ce_{0.5}Zr_{0.5}O₂ exhibits significantly larger activity. In particular, at 200 °C the conversion of C₃H₆ is 30% for Pd/Ce_{0.5}Zr_{0.5}O₂, while after deposition of P, P-Ca, or P-Zn it is decreased to the value of 2, 8 and 10%, respectively. At 290 °C, Pd/Ce_{0.5}Zr_{0.5}O₂ exhibits a propylene conversion of 52%, which is two times higher than that obtained over the contaminated samples. In addition, for the latter samples, complete C₃H₆ conversion is achieved at higher reaction temperatures (T > 550 °C), whereas for the Pd/Ce_{0.5}Zr_{0.5}O₂ solid, full conversion is attained at ~480 °C.

Fig. 9b presents the TPSR profile of X_{NO} (%) (dependence of NO conversion on reaction temperature, 30–700 °C) for the

reduction of NO by H₂ in the presence of oxygen (0.1 vol% NO/0.3 vol%H₂/1 vol%O₂/He) over the Pd/Ce_{0.5}Zr_{0.5}O₂-aged solid and that after contamination with P, P-Ca or P-Zn. The results show that all catalysts are active in the lean deNO_x reaction. The reduction of NO by hydrogen in the presence of oxygen was found to result mainly in the production of H₂O and N₂. It was estimated that the N₂-selectivity of NO reduction was ~97%, and only up to 30 ppm of N₂O was produced, whereas NH₃ and NO₂ were not detected at the exit of the micro-reactor. As seen in Fig. 9b, higher conversions are measured over the non-contaminated Pd/Ce_{0.5}Zr_{0.5}O₂ catalyst, especially at $T > 200$ °C. In particular, at 250 and 480 °C the X_{NO} obtained prior to chemical poisoning is 68%, which is also the maximum NO conversion observed, whereas this is reduced by half after poisoning (X_{NO} = 30–35% for all the contaminated samples). The highest NO conversion attained over the contaminated samples was about 50% at ~125 °C. It should be noted that complete conversion of NO was not achieved. This could be explained by considering that the present Pd-based catalyst does not contain Rh, which is widely recognized as an effective catalytic component for NO reduction [60,61]. Adamowska et al. [61] found that the conversion of NO_x to N₂ depends on the reducibility of Ce_xZr_{1-x}O₂ solid, and suggested that the deNO_x conversion is controlled by the ability of oxygen vacancies formation, leading to “co-ordinatively unsaturated sites” (“cus”), thus permitting NO adsorption via the participation of Ce³⁺-□-Ce³⁺ active sites. H₂-TPR studies previously reported by us [30] showed that the addition of P, Ca and Zn poisons on the present Ce_{0.5}Zr_{0.5}O₂ solid hinders the surface shell reduction of Ce_{0.5}Zr_{0.5}O₂ solid, which in turn prevents triggering of bulk oxygen diffusion. Since oxygen mobility is significantly restricted on the surface of support particles [30], where CePO₄ is formed after the incorporation of P, the catalyst performance is found to be significantly deteriorated towards CO and C₃H₆ oxidation and NO reduction by hydrogen.

It is very important to state here that the comparison of TPSR profiles of the various catalysts in Figs. 8b and 9 are not largely due to internal mass transport (diffusion) effects due to appreciable differences in the pores structure of the catalysts (Table 2). If this was the case, then at the high-temperature range of 400–700 °C, where gas diffusion is expected to become more important than at lower temperatures, the X_{CO} would have been expected to present significant differences. However, the opposite was observed. Therefore, the large differences in activity especially observed at $T < 400$ °C in the presence of the various contaminants on Pd/Ce_{0.5}Zr_{0.5}O₂ is a true chemical effect.

4. Conclusions

The following main conclusions can be derived from the results of the present work:

- (a) Contamination of a 1 wt% Pd/Ce_{0.5}Zr_{0.5}O₂ solid by P followed by calcination at 850 °C was found to result in the formation of CePO₄ on the surface and upper subsurface layers of the solid. Upon co-addition of Ca or Zn with P, these two contaminants were also found to highly accumulate on the surface of the solid in the form of Ca₃(PO₄)₂ and ZnO, respectively.
- (b) Deposition of P, Ca and Zn contaminants on the surface of a 1 wt% Pd/Ce_{0.5}Zr_{0.5}O₂ solid induces a significant loss in its surface area (50–67%) and pores volume (40–69%) due to chemical structural transformations that lead to the formation of new solid phases in the catalyst, causing its pores structure to partly collapse and clogging its pore's mouth. Palladium surface sites measured by selective hydrogen chemisorption were also found to decrease significantly after incorporation of P and Ca, and especially when P and Zn were co-added. This apparent decrease of Pd

dispersion is not due to any thermal sintering effect but to the partial covering of Pd surface by the contaminants.

- (c) XPS results strongly support the fact that after P-poisoning of Pd/Ce_{0.5}Zr_{0.5}O₂, support oxygen binds to phosphorus forming phosphate salts (e.g., CePO₄ as evidenced by XPD), at least in the surface and upper subsurface region of the catalyst. Since Pd local electronic environment was found not to be affected by the presence of P, Ca or Zn contaminants, it is speculated that compounds made of the latter species mainly accumulate on the surface of Pd/Ce_{0.5}Zr_{0.5}O₂, which physically block the surface of a large number of Pd and Ce_{0.5}Zr_{0.5}O₂ primary crystal particles, therefore, catalytic active sites.
- (d) Deposition of P, P-Ca and P-Zn contaminants on the surface of 1 wt% Pd/Ce_{0.5}Zr_{0.5}O₂ catalyst was found to lead to a considerable deterioration of its oxygen storage and release properties. At temperatures lower than 650 °C, the concentration of labile oxygen species (OSC) was found to be more influenced by the presence of P-Zn poisons (up to 40% loss), which is in accordance to the lower Pd surface sites concentration measured, as well as the dramatic loss in BET area and pores volume observed. At $T > 650$ °C, the OSC and OSCC values were reduced by 170–450 μmol O/g_{cat} after P-poisoning (16–28% loss), while no further reduction was observed after depositing Zn or Ca with P. This result is in agreement with the fact that the degree of reduction of Ce(IV) oxide after P-poisoning was found to be significantly reduced, and it was the same for the three contaminated samples.
- (e) The oxygen storage capacity was found to be up to 10 times higher over the contaminated supported-Pd catalysts investigated here, compared to the respective Ce_{0.5}Zr_{0.5}O₂ contaminated samples [30]. It is thus clear that the presence of Pd on the surface of Ce_xZr_{1-x}O₂ support causes the reduction to a considerable degree of the deactivating effects of P, Ca and Zn on the oxygen storage and release properties of Ce_{0.5}Zr_{0.5}O₂, most likely through the promotion of hydrogen dissociation and activation steps, and that of the back-spillover of oxygen from Ce_{0.5}Zr_{0.5}O₂ to the oxygen vacant sites of surface Pd in its reduced state.
- (f) The catalytic performance in terms of CO, C₃H₆ and NO conversions is considerably reduced upon contamination of Pd/Ce_{0.5}Zr_{0.5}O₂ with P, P-Ca or P-Zn. Evaluation of catalytic activity for CO and C₃H₆ oxidation and NO reduction by H₂ revealed that the deactivation trend followed by P, P-Ca and P-Zn chemical poisoning is similar. It can be thus concluded that the presence of Ca and Zn does not lead to further worsening of the concerned catalytic activity of Pd/Ce_{0.5}Zr_{0.5}O₂ model “three-way” catalyst compared to that obtained after P-poisoning alone. This is due to the formation of CePO₄, which binds a large amount of catalyst's active oxygen.

Acknowledgments

The financial support of the Cyprus Research Promotion Foundation through the project ΔΙΔΑΚΤΩΡ/ΔΙΣΕΚ/0308/33 is gratefully acknowledged. The authors also thank MEL Chemicals (Manchester, UK) for providing the Ce_{0.5}Zr_{0.5}O₂ support material.

References

- [1] M. Shelef, K. Otto, N.C. Otto, *Adv. Catal.* 27 (1979) 311.
- [2] C.H. Bartholomew, *Appl. Catal. A: Gen.* 212 (2001) 17.
- [3] F.M. Zanon Zotin, O.F. Martins Gomes, C.H. de Oliveira, A.A. Neto, M.J. Baldini Cardoso, *Catal. Today* 107–108 (2005) 157.
- [4] T.N. Angelidis, M.M. Koutlemani, S.A. Sklavounos, Ch.B. Lioutas, A. Voulgaropoulos, V.G. Papadakis, H. Emons, *Stud. Surf. Sci. Catal.* 116 (1998) 155.
- [5] U. Lassi, R. Polvinen, S. Suhonen, K. Kallinen, A. Savimäki, M. Härkönen, M. Valden, R.L. Keiski, *Appl. Catal. A: Gen.* 263 (2004) 241.

[6] L. Martín, L.L. Arranz, O. Prieto, R. Trujillano, M.J. Holgado, M.A. Galán, V. Rives, *Appl. Catal. B: Environ.* 44 (2003) 41.

[7] W.B. Williamson, J. Perry, H.S. Gandhi, J.L. Bomback, *Appl. Catal.* 15 (1985) 277.

[8] M. López Granados, F. Cabello Galisteo, R. Mariscal, M. Alifanti, A. Gurbani, J.L.G. Fierro, R. Fernández-Ruiz, *Appl. Surf. Sci.* 252 (2006) 8442.

[9] S.Y. Christou, H. Birgersson, A.M. Efstatou, *Appl. Catal. B: Environ.* 71 (2007) 185.

[10] V. Kröger, U. Lassi, K. Kynkänniemi, A. Suopanki, R.L. Keiski, *Chem. Eng. J.* 120 (2006) 113.

[11] L. Xu, G. Guo, D. Uy, A.E. O'Neill, W.H. Weber, M.J. Rokosz, R.W. McCabe, *Appl. Catal. B: Environ.* 50 (2004) 113.

[12] C. Larese, F.C. Galisteo, M.L. Granados, R. Mariscal, J.L.G. Fierro, M. Furió, R.F. Ruiz, *Appl. Catal. B: Environ.* 40 (2003) 305.

[13] C. Larese, M. López Granados, F. Cabello Galisteo, R. Mariscal, J.L.G. Fierro, *Appl. Catal. B: Environ.* 62 (2006) 132.

[14] T. Tabata, H. Kawashima, K. Baba, *Stud. Surf. Sci. Catal.* 111 (1997) 259.

[15] T. Tabata, K. Baba, H. Kawashima, *Appl. Catal. B: Environ.* 7 (1995) 19.

[16] D.D. Beck, J.W. Sommers, *Stud. Surf. Sci. Catal.* 96 (1995) 721.

[17] D.R. Monroe, M.H. Krueger, D.D. Beck, M.J. D'Aniello Jr., *Stud. Surf. Sci. Catal.* 71 (1991) 593.

[18] M.L. Granados, C. Larese, F.C. Galisteo, R. Mariscal, J.L.G. Fierro, R. Fernandez-Ruiz, R. Sanguino, M. Luna, *Catal. Today* 107–108 (2005) 77.

[19] T.N. Angelidis, S.A. Sklavounos, *Appl. Catal. A: Gen.* 133 (1995) 121.

[20] C. Battistoni, V. Cantelli, M. Debenedetti, S. Kaciulis, G. Mattogno, A. Napoli, *Appl. Surf. Sci.* 114–115 (1999) 390.

[21] D.R. Liu, J.S. Park, *Appl. Catal. B: Environ.* 2 (1993) 49.

[22] M.J. Rokosz, A.E. Chen, C.K. Lowe-Ma, A.V. Kucherov, D. Benson, M.C. Paputa Peck, R.W. McCabe, *Appl. Catal. B: Environ.* 33 (2001) 205.

[23] A.J. Oakes, J.C. Vickerman, *Surf. Interf. Anal.* 24 (1996) 695.

[24] C. Larese, F.C. Galisteo, M.L. Granados, R.M. López, J.L.G. Fierro, P.S. Lambrou, A.M. Efstatou, *Appl. Catal. B: Environ.* 48 (2004) 113.

[25] C. Larese, F.C. Galisteo, M.L. Granados, R. Mariscal, J.L.G. Fierro, P.S. Lambrou, A.M. Efstatou, *J. Catal.* 226 (2004) 443.

[26] C. Larese, M.L. Granados, R. Mariscal, J.L.G. Fierro, P.S. Lambrou, A.M. Efstatou, *Appl. Catal. B: Environ.* 59 (2005) 13.

[27] M.L. Granados, F.C. Galisteo, P.S. Lambrou, M. Alifanti, R. Mariscal, A. Gurbani, J. Sanz, I. Sobrados, A.M. Efstatou, J.L.G. Fierro, *Top. Catal.* 42–43 (2007) 443.

[28] V. Kröger, M. Hietikko, U. Lassi, J. Ahola, K. Kallinen, R. Laitinen, R.L. Keiski, *Top. Catal.* 30–31 (2004) 469.

[29] I. Heo, J.W. Choung, P.S. Kim, I.-S. Nam, Y.I. Song, *Appl. Catal. B: Environ.* 92 (2009) 114.

[30] S.Y. Christou, M.C. Álvarez-Galván, J.L.G. Fierro, A.M. Efstatou, *Appl. Catal. B: Environ.* 106 (2011) 103.

[31] C.N. Costa, T. Anastasiadou, A.M. Efstatou, *J. Catal.* 194 (2000) 250.

[32] C.D. Wagner, L.E. Davis, M.V. Zeller, J.A. Taylor, R.H. Raymond, L.H. Gale, *Surf. Interf. Anal.* 3 (1981) 211.

[33] H.C. Yao, Y.F. Yu Yao, *J. Catal.* 86 (1984) 254.

[34] P.S. Lambrou, C.N. Costa, S.Y. Christou, A.M. Efstatou, *Appl. Catal. B: Environ.* 54 (2004) 237.

[35] C.N. Costa, P.G. Savva, C. Andronikou, P. Lambrou, K. Polychronopoulou, V.C. Belessi, V.N. Stathopoulos, P.J. Pomonis, A.M. Efstatou, *J. Catal.* 209 (2002) 456.

[36] L.F. Liotta, A. Macaluso, A. Longo, G. Pantaleo, A. Martorana, G. Deganello, *Appl. Catal. A: Gen.* 240 (2003) 295.

[37] A. Kambolis, H. Matralis, A. Trovarelli, Ch. Papadopoulou, *Appl. Catal. A: Gen.* 377 (2010) 16.

[38] L. Karpowich, R. Yu, G. Harley, J.A. Reimer, L.C. De Jonghe, *J. Sol. State Chem.* 180 (2007) 840.

[39] D.M. Fernandes, C.F. Scofield, A.A. Neto, M.J. Baldini Cardoso, F.M. Zanon Zotin, *Chem. Eng. J.* 160 (2010) 85.

[40] D.R. Monroe, SAE Technical Paper No. 800859 (1980).

[41] M. Fuchs, B. Jenewein, S. Penner, K. Hayek, G. Rupprechter, D. Wang, R. Schlägl, J.J. Calvino, S. Bernal, *Appl. Catal. A: Gen.* 294 (2005) 279.

[42] S. Bernal, J.J. Calvino, M.A. Caquici, J.M. Gatica, C. López Cartes, L.A. Pérez Omil, J.M. Pintado, *Catal. Today* 77 (2003) 385.

[43] A. Trovarelli, C. de Leitenburg, M. Boaro, G. Dolcetti, *Catal. Today* 50 (1999) 353.

[44] E.W. Shin, S.-I. Cho, J.H. Kang, W.J. Kim, J.D. Park, S.H. Moon, *Korean J. Chem. Eng.* 17 (2000) 468.

[45] V. Ragaini, R. Giannantonio, P. Magni, L. Lucarelli, G. Leofanti, *J. Catal.* 146 (1994) 116.

[46] N. Hickey, P. Fornasiero, J. Kašpar, J.M. Gatica, S. Bernal, *J. Catal.* 200 (2001) 181.

[47] P.S. Lambrou, A.M. Efstatou, *J. Catal.* 240 (2006) 182.

[48] S.Y. Christou, A.M. Efstatou, *Top. Catal.* 42–43 (2007) 351.

[49] S.-Y. Wang, S.H. Moon, M.A. Vannice, *J. Catal.* 71 (1981) 167.

[50] C.D. Wagner, W.M. Riggs, L.E. Davis, J.F. Moulder, "Handbook of X-ray Photoelectron Spectroscopy", Physical Electron Division C, 1995.

[51] J.M. Pemba-Mabiala, M. Lenzi, J. Lenzi, A. Lebugle, *Surf. Interf. Anal.* 15 (1990) 663.

[52] B. Demri, D. Muster, J. Mater. Process. Tech. 55 (1995) 311.

[53] F. Guodong, F. Changgen, Z. Zhao, *J. Rare Earths* 25 (2007) 42.

[54] P. Burroughs, A. Hamnett, A.F. Orchard, G. Thornton, *J. Chem. Soc. Dalton Trans.* 17 (1976) 1686.

[55] E. Paparazzo, *Appl. Catal. B: Environ.* 105 (1–2) (2011) 248.

[56] Y. Madier, C. Descorme, A.M. Le Govic, D. Duprez, *J. Phys. Chem. B* 103 (1999) 10999.

[57] L.F. Chen, G. González, J.A. Wang, L.E. Noreña, A. Toledo, S. Castillo, M. Morán-Pineda, *Appl. Surf. Sci.* 243 (2005) 319.

[58] S. Bedrane, C. Descorme, D. Duprez, *Catal. Today* 75 (2002) 401.

[59] J.H. Baik, H.J. Kwon, Y.T. Kwon, I.-S. Nam, S.H. Oh, *Top. Catal.* 42–43 (2007) 337.

[60] K.C. Taylor, *Catal. Rev. Sci. Eng.* 35 (1993) 457.

[61] M. Adamowska, A. Krzton, M. Najbar, P. Da Costa, G. Djega-Mariadassou, *Catal. Today* 137 (2008) 288.